Coordination chemistry of neutral mono-oxide, sulfide and selenide bis(diphenylphosphino)amine (DPPA)-based ligands and their N-substituted/functionalized derivatives

Christophe Fliedel, Rinaldo Poli

Coordination chemistry of neutral mono-oxide, sulfide and selenide bis(diphenylphosphino)amine (DPPA)-based ligands and their *N*-substituted/functionalized derivatives.

Christophe Fliedel[a]* and Rinaldo Poli[a,b]

[a] Laboratoire de Chimie de Coordination (LCC), CNRS-UPR 8241, Université de Toulouse, UPS, INPT, 205 Route de Narbonne, Toulouse F-31077 Cedex 4, France

[b] Institut Universitaire de France, 1 Rue Descartes, 75231 Paris, Cedex 05, France

Corresponding author: christophe.fliedel@lcc-toulouse.fr

Dedication.

Dedicated to our friend and colleague, Pierre Braunstein, on the occasion of his 70th birthday, with our most sincere congratulations and best wishes.

Abstract.

This review provides a summary, including spectroscopic and structural data, of the metal complexes accessible with mono-oxide, sulfide and selenide bis(diphenylphosphino)amine (DPPA)-based ligands and their *N*-substituted/functionalized derivatives. The nature of the E (O, S ,Se) donor in these mixed *P*,P=*E* donor ligands strongly influences the nature of the resulting metal complexes, which can incorporate the DPPA-type ligand(s) as *P*-monodentate or *P*,*E*-chelate. When available, a comparison between the reactivity of the mixed *P*,P=*E* and parent *P*,*P* systems is given. The catalytic applications of *P*,*E*-supported metal complexes are also discussed.

Keywords.

Aminophosphine – Phosphine oxide – Hybrid ligands – Chelating ligands – Transition metal complexes – Catalysis

Abbreviations:

allyl, η^3-CH_2CHCH_2;

av, average;

COD, 1,5-cyclooctadiene;

Cp, η^5-C_5H_5;

Cp*, η^5-C_5Me_5;

DME, 1,2-dimethoxyethane;

DPPA, bis(diphenylphosphino)amine;

DPPM, bis(diphenylphosphino)methane;

eq, equivalent;

FT-IR, Fourier transform infrared spectroscopy;

methallyl, η^3-$CH_2C(CH_3)CH_2$;

p-Cym, η^5-*p*-(Me)C_6H_4(^{i}Pr);

Pip, $C_5H_{11}N$ (Piperidine);

RT, room temperature;

XRD, X-ray diffraction;

NOTE: Unless otherwise specified, ^{31}P and ^{13}C refer to decoupled $^{31}P\{^1H\}$ and $^{13}C\{^1H\}$ NMR experiments.

Contents

1. Introduction

Coordination/organometallic complexes hold a leading position in many areas of Chemistry, including for example homogeneous and heterogeneous catalysis, the development of high-tech materials or therapeutic molecules and photophysical chemistry. However, the development of suitable candidates for these applications is, in most cases, related to an appropriate design of the supporting ligand(s). In this context, short-bite ligands, such as bis(diphenylphosphino)amine (**DPPA**, Scheme 1) [1-3] or bis(diphenylphosphino)methane (**DPPM**), have attracted much attention for their ability to bring in close proximity two identical or different metal centers, allowing metal-metal interactions [4-14] or cooperative effects [15]. Derivation of these ligands by mono- or bis-oxidation do not only affect the bite-angle of the resulting chelating ligands, from 4- to 5- or 6-membered metallocycles, respectively. The presence of different chemical functions, which might be a combination of hard and soft donors, in such heterotopic/hybrid ligands within the same molecule may generates hemilabile systems [16-19]. Consequently, the weak chelation may facilitate the generation of (re)active and/or coordinatively unsaturated species and lower the activation energy of metal-mediated transformations [20-22].

The (coordination) chemistry of **DPPA** and related ligands, such as **DPPM** or other aminophosphines (P-N bond containing molecules), was the subject of several reviews [1-3, 23]. A certain interest in the mono-anionic **DPPA**$_{\text{-H}}^{-}$ ligand (Scheme 1), resulting from the deprotonation of the N-*H* group of **DPPA**, and analog ligands (varying the P-substituents) could be evidenced by a couple of review articles [24-26]. A comprehensive review dedicated to the synthesis, coordination chemistry and applications of **DPPA**-type ligands, functionalized on the N atom by an additional chemical function (*e.g*. amine, (thio)ether, phosphine, Scheme 1) was recently provided by Fliedel, Ghisolfi and Braunstein [27].

We were interested in providing a survey of the coordination chemistry of neutral mono- (**DPPA-E**) and homo- and hetero-bis-oxide (P=O), sulfide (P=S) and selenide (P=Se) (**DPPA-EE'**) bis(diphenylphosphino)amine-based ligands and their *N*-substituted/functionalized derivatives (Scheme 1, insets). The present review has been restricted to mono-oxidized systems (Scheme 1, solid inset), while a following report will be dedicated to recent work on bis-oxidized systems (Scheme 1, dashed inset) [28]. The influence of 1) the nature of the P=*E* donor, and 2) the substitution of the N-*H* group by a hydrocarbyl or heteroatom-containing group will be highlighted, based (especially) on NMR and structural data. The reactivity and applications of the resulting complexes is also discussed. However, coordination compounds in which the ligand(s) will be deprotonated (**DPPA-E**$_{\text{-H}}^{-}$ in Scheme 1) are outside the scope of this review, which will focus on metal complexes supported by neutral **DPPA-E** ligands and their *N*-substituted derivatives. Our objective is to provide the researchers studying the coordination chemistry of such **DPPA-E**-type ligands a rapid and comprehensive access to the characteristic spectroscopic and structural data available for all complexes reported to date.

The coordination chemistry of bis-oxidized **DPPA-EE'** (E = O, S, Se) [26], and derivatives in which the P*Ph* was replaced by other aryl, alkyl, or OR groups, has been overviewed in 1998 [29] and 2001 [30], but mostly concern metal complexes in which the ligands are deprotonated. As mentioned above, we will shortly provide an update on the coordination chemistry of neutral bis-oxidized **DPPA-EE'** (E = O, S, Se) ligands and their *N*-substituted derivatives, which will be complementary to the latter reviews [28]. The access to mixed phosphine-phosphine oxide ligands, their coordination chemistry and the catalytic applications of the resulting metal complexes, was thoroughly reviewed in the mid 2000's by Grushin [31]. However, **DPPA-O** and its derivatives were not discussed in that review.

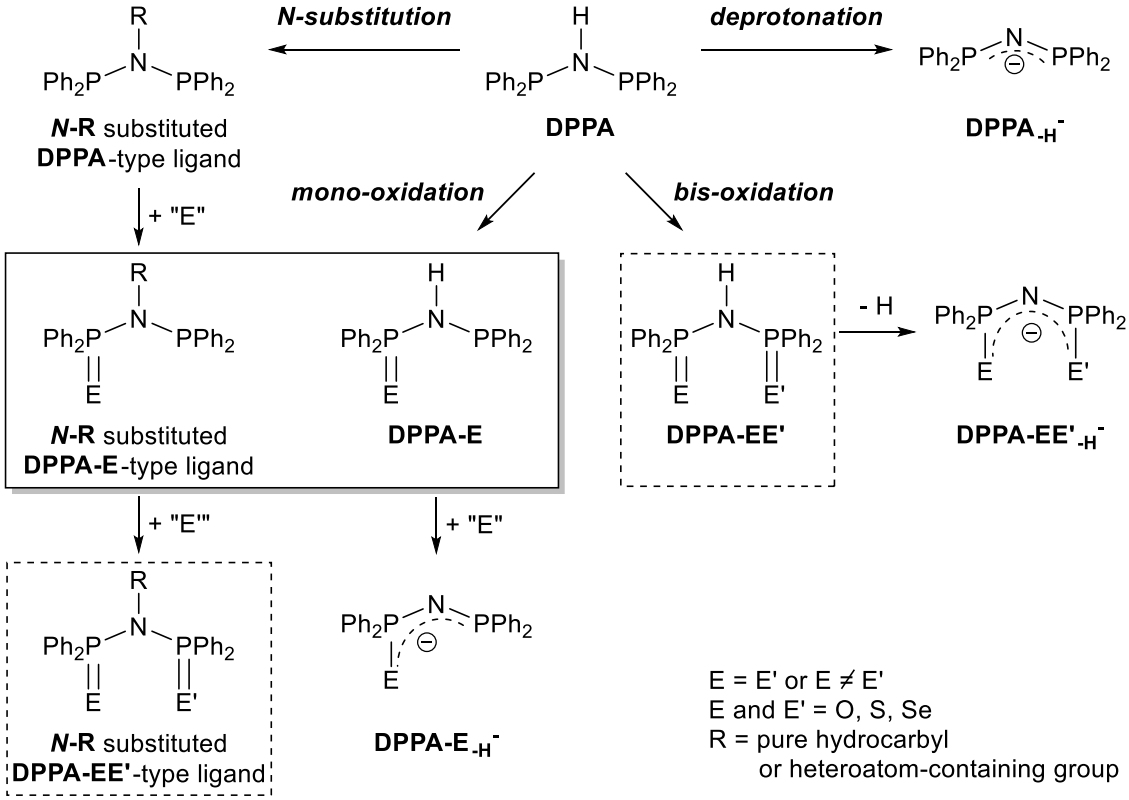

Scheme 1. Bis(diphenylphosphino)amine (DPPA) ligand and its derivatives. The solid inset highlight the ligands topic of this review, and the dashed inset mark the subject of our complement report [28].

2. DPPA mono-oxide (**DPPA-O**)

Woolins and co-workers reported the synthesis, isolation and characterization of the mixed P^{III}/P^{V} ligand **DPPA-O**, the mono-oxide derivative of **DPPA**, in the second half of the 90's (Scheme 2) [32, 33]. **DPPA-O** was obtained by treatment of **DPPA** with H_2O_2 as oxidizing agent. The moderate yield obtained (*ca*. 49%) is due to the concomitant formation of the bis-oxide derivative (**DPPA-O$_2$**, see section 6), even at low temperature (THF, -20°C). However, the lower solubility of the latter in THF allowed its separation. Ligand **DPPA-O** exhibits a characteristic ^{31}P NMR spectrum, containing two doublets centered at 28.1 (P^{III}) and 21.3 ppm (P^{V}) with a $^{2}J_{P,P=O}$ coupling constant of 62 Hz (Table 1). The integrity of the N-H moiety is shown by a characteristic *ν*(N-H) broad absorption band at 3031 cm^{-}

[1] in the FT-IR spectrum of **DPPA-O**. Moreover, H-bonds involving the N-*H* and P=*O* moieties of two **DPPA-O** molecules are present in the solid-state, resulting in the formation of OPNHOPNH macrocycles (Figure 1). Characteristic structural data are summarized in Table 1.

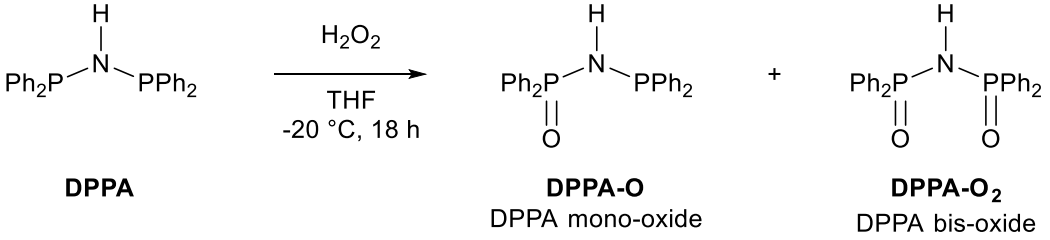

Scheme 2. Preparation of **DPPA-O** by oxidation of **DPPA**. The bis-oxide **DPPA-O$_2$** side product is removed by filtration (insoluble in THF) [32, 33].

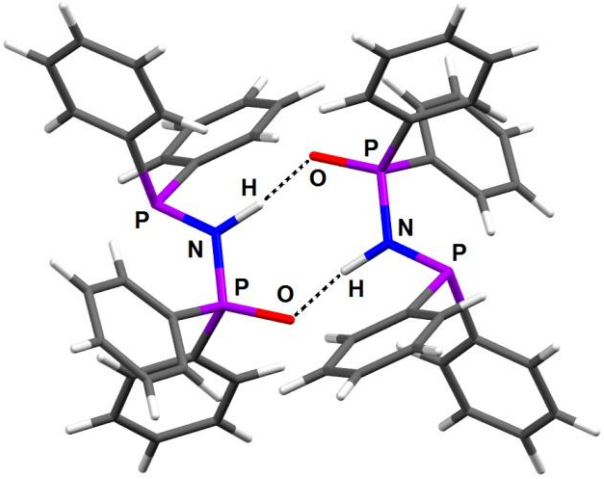

Figure 1. Solid-state structure of **DPPA-O** showing the H-bond between the P=*O* and N-*H* moieties [33].

2.1. Group 10 metal complexes

Group 10 metal complexes, including phosphine-stabilized species, are of great interest because of their multiple applications. Palladium complexes were extensively studied for their exceptional performances in catalysis, especially in cross-coupling reactions [34-36], and direct C-H functionalization/arylation [34, 37, 38], and continuing effort are devoted to develop new efficient catalysts for these transformations. Moreover, phosphine-containing palladium and nickel complexes found a niche in the field of olefin oligo/polymerization and co-polymerization with CO [27, 39-41]. Platinum complexes are well established in the photophysics and photochemistry areas for their unique luminescent properties [9, 12, 42]. More recently, platinum-catalyzed organic transformations, including by C-H functionalization, gained increasing interest [42-44].

Reaction between isolated **DPPA-O** and the dimeric [(allyl)Pd (μ-Cl)]$_2$ precursor led to a cleavage of the chloride bridges and the formation of the mononuclear [(allyl)PdCl(**DPPA-O**)-*P*)] complex **1** (Scheme 3) [32]. In the latter, **DPPA-O** acts as a monodentate ligand, binding the metal center only through the phosphine ligand. As a result, the ^{31}P NMR resonance of the P^{III} atom is strongly downfield shifted compared to the free ligand ($\Delta\delta$ = 32.8 ppm), while the P^{V} resonance was only slightly affected (Table 1). For all Group 10 metal complexes of **DPPA-O**, both P^{III} and P^{V} resonances appear as doublets, which originate from an AX spin system, with $J_{P,P=O}$ couplings ranging from 3 to 37 Hz (Table 1). Chelation of **DPPA-O** can be forced by a chloride abstraction reaction, using $AgBF_4$ in CH_2Cl_2, affording the mononuclear cationic complex [(allyl)Pd(**DPPA-O**)-*P*,*O*)][BF_4] (**2**, Scheme 3). The formation of a five-membered PdPNPO metallacycle could be confirmed in the solid-state by XRD analysis. Both P-N (av) and P=O bond lengths were not significantly affected by the coordination of the Pd center, while the PNP angle was found slightly more acute in **2** compared to free **DPPA-O** (Table 1). In contrast to **1**, the ^{31}P NMR spectrum of **2** exhibits two doublets in the same (low field) region (Table 1). In the FT-IR spectra of complexes **1** and **2** a characteristic ν(N-H) absorption band at 3134 and 3180 cm^{-1}, respectively, confirms the absence of N-H deprotonation and the neutral nature of the ligand.

Similarly, the [(methallyl)Ni (**DPPA-O**)-*P*,*O*)][SbF_6] (**3**) complex was prepared by a two-steps one-pot procedure that involves 1) a bridge cleavage reaction of [(methallyl)Ni (μ-Br)]$_2$ with 2 eq. **DPPA-O**, followed by 2) a bromide abstraction using $AgSbF_6$ (Scheme 3) [45]. In solution, the Ni^{II} complex **3** probably adopts a (distorted) square-planar geometry, resulting in a diamagnetic species, which exhibits a ^{31}P NMR spectrum comparable to that of the closely related Pd^{II} complex **2** (Table 1). The N-*H* resonance could be observed, as a broad singlet at 5.74 ppm, in the ^{1}H NMR spectrum of **3**. The Ni^{II} complex **3**, along with other cationic Ni^{II} complexes of mixed P/P=O chelating ligands, were evaluated in the catalytic oligomerization of ethylene [45]. All complexes are efficient catalyst precursors for the oligomerization of ethylene to linear, higher α-olefins. However, the moderate selectivity to α-olefins in the case of **3** (53%) highlights that the latter is also an efficient catalyst for the isomerization of α-olefins to internal olefins. The authors highlighted that the maximum chain length of produced olefins increased with decreasing the chelate ring size of the complex (5- to 7-membered metallocycles were studied).

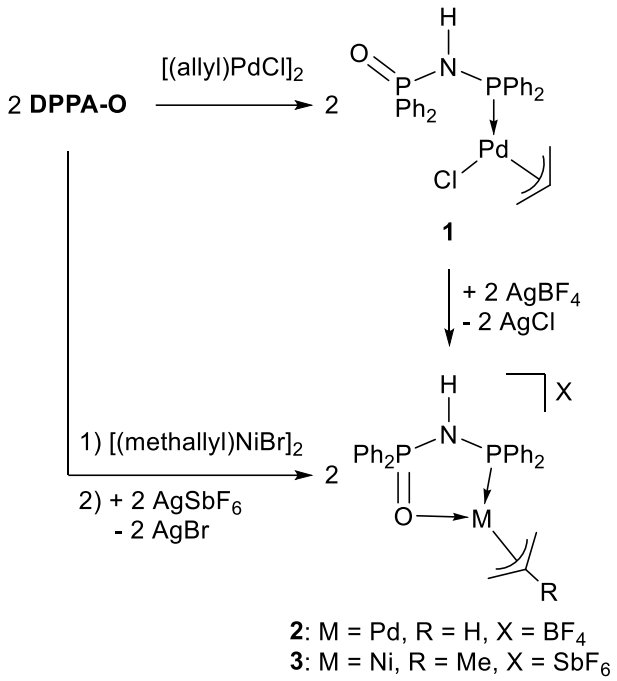

Scheme 3. Reactivity of **DPPA-O** towards the [(allyl)Pd (μ-Cl)]$_2$ and [(methallyl)Ni (μ-Br)]$_2$ precursors [32, 45].

The coordination chemistry of the mixed P^{III}/P^{V} ligand **DPPA-O** towards bis-halo or halo/alkyl palladium and platinum precursors was extensively studied by Woolins and co-workers [33]. The authors demonstrated that ligand **DPPA-O** readily reacts with [MXY(COD)] (M = Pd, Pt; X and Y = Cl, Br, I, Me) precursors, in a 2:1 ligand/metal ratio, to afford the tetracoordinated [MXY{(**DPPA-O**)-*P*}$_2$] (**4**-**5** and **7**-**10**) by substitution of the labile COD ligand by two P donors of two **DPPA-O** ligands (Scheme 4). These compounds were obtained as pure *cis*- (**7**, **8**) or *trans*- (**5**, **6**, **10**, **11**) isomer or as mixtures of both in variable proportions [*cis*/*trans* = 1:3.7 (**4**) and 1:1.2 (**9**)] as deduced by ^{31}P NMR (Table 1). Successful halide exchange, from Cl to I, was performed by treatment of **4** (Pd) or **10** (Pt) with excess NaI, affording **6** (Pd) or **11** (Pt), respectively.

The ^{31}P NMR resonance of the PPh_2 fragment of the **DPPA-O** ligand was strongly affected upon coordination to the Pd^{II} centers in complexes **4**-**6** ($17.6 < \Delta_\delta < 30.5$ ppm), while the P=O resonance remained nearly unchanged, supporting non-coordination of the latter (Table 1). Moreover, the P^{III} resonance of the *cis*-isomer of **4** was significantly more downfield shifted compared to those of the *trans* species [δ 58.3 (**4**-*cis*) *vs.* ≈ 47 (**4**-*trans*-**6**) ppm, Table 1].

The ^{31}P NMR spectra of the Pt^{II} complexes exhibited, as expected, two doublets for the non-equivalent P^{III} and P^{V} centers. However, both are flanked by typical $^{1}J_{P,Pt}$ and $^{3}J_{P=O,Pt}$ satellites, which significantly vary as a function of the ligands arrangement (*cis*/*trans*, Table 1) [33]. Similarly to their palladium analogs, the ^{31}P NMR resonance of the PPh_2 fragment in the platinum dihalide complexes (**7**-**9**) was downfield shifted compared to the free **DPPA-O** ligand ($\Delta\delta$ = 8-10 ppm), but without significant

difference between *cis* and *trans* isomer (Table 1). The P=O moiety in **7**-**9** resonates in a similar range than the free **DPPA-O** ligand. The ^{31}P NMR spectra of the mixed halide/alkyl Pt^{II} complexes (**10**-**11**) are very similar to those of their dihalide analogs (**7**-**9**). However, the chemical shift of the coordinated PPh_2 moiety are more strongly downfield shifted (*ca*. 20 ppm) and the $J_{P,P=O}$ coupling constants are weaker (Table 1).

The solid-state structures of complexes **7** (*cis*) and **10** (*trans*) could be established by XRD analyses, which confirmed a slightly distorted square planar geometry around the Pt^{II} center [33]. The uncoordinated P=O bond lengths were slightly shorter than in the free **DPPA-O** ligand, while the P-N ones were nearly unaffected (Table 1). In contrast to the *P*,*O*-chelate complex **2** [PNP = 120.8(4)°], the PNP bond angles in **7** and **10** (131.5°), were found larger than in the free ligand [125.6(2)°].

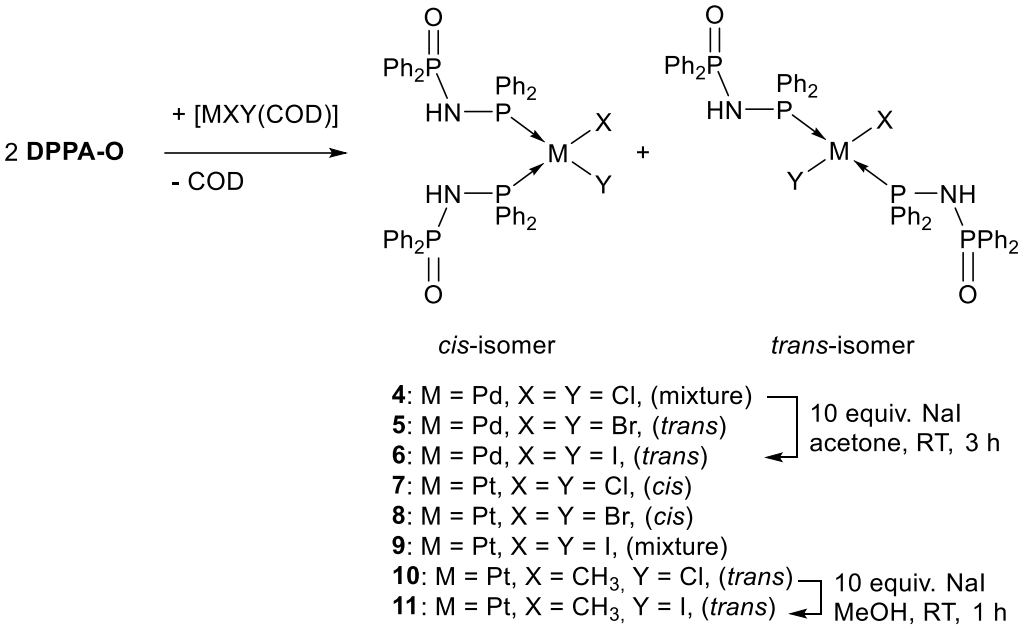

Scheme 4. Group 10 metal complexes of **DPPA-O** [33].

As shown for the transformation of **1** to **2** (Scheme 3), the chelation of the **DPPA-O** ligand can be favored by ionization of the parent complexes, *i.e*. **4** ($PdCl_2$) or **7** ($PtCl_2$), using a silver salt ($AgBF_4$) as chloride abstractor, to afford the dicationic bis-chelated *cis*-[M{(**DPPA-O**)-*P*,*O*}$_2$][BF_4]$_2$ [M = Pd (**12**), Pt (**13**)] complexes (Scheme 5). The ^{31}P NMR resonance of the P=O moiety of the **DPPA-O** ligand was significantly downfield shifted upon coordination in **12** and **13** compared to **4** and **7**, from *ca*. 21 ppm to 68.1 and 62.8 ppm, respectively (Table 1). In contrast, the neutral or cationic nature of the metal complexes does not affect much the ^{31}P NMR resonance of the PPh_2 moiety ($\Delta\delta \leq 2$ ppm , Table 1). The *cis* arrangement of the **DPPA-O** ligands and the slightly distorted square planar coordination geometry around the metal center could be established by XRD in the case of the Pt^{II} complex **13** (Table 1 and Figure 2). Both P-N and P=O bond lengths were found in the same range than in the free **DPPA-O** ligand, while the PNP angle imposed by the metal coordination was much more acute [118.1(7) *vs*.

125.6(2)°]. The other structural parameters involving the Pt^{II} metal center were found closely related those of the cationic *P*,*O*-chelate Pd^{II} complex **2** (Table 1).

The authors reported an alternative route to the formation of the dicationic bis-*P*,*O*-chelated complexes **12**-**13** [33]. This pathway involves in a first step the deprotonation of the **DPPA-O** N-*H* moiety by a strong base in **4** and **7**, to afford the neutral bis-*P*,*O*-chelated complexes **12a**-**13a** (not the topic of this review). The latter can then be selectively re-protonated with HBF_4•OEt_2 to form complexes **12**-**13** nearly quantitatively (Scheme 5). Cationic (**12**-**13**) and neutral bis-*P*,*O*-chelated complexes (**12a**-**13a**) can readily be inter-converted through deprotonation/re-protonation reactions. The reactivity/acidity of the N-*H* fragment was also illustrated by the room temperature deprotonation of the transient *cis*-[$Pt(CH_3)_2${(**DPPA-O**)-*P*}$_2$] complex (**14**, Table 1), resulting from the reaction between [$Pt(CH_3)_2$(COD)] and **DPPA-O** (1:2 molar ratio), which afforded complex **13a** and CH_4 (2 eq.) [33].

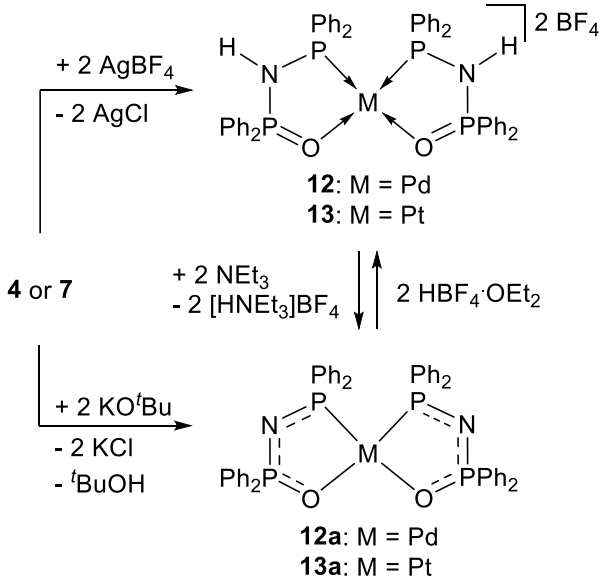

Scheme 5. Formation of dicationic Pd^{II} and Pt^{II} complexes (**12**-**13**) of **DPPA-O** in *P*,*O*-chelate coordination mode [33].

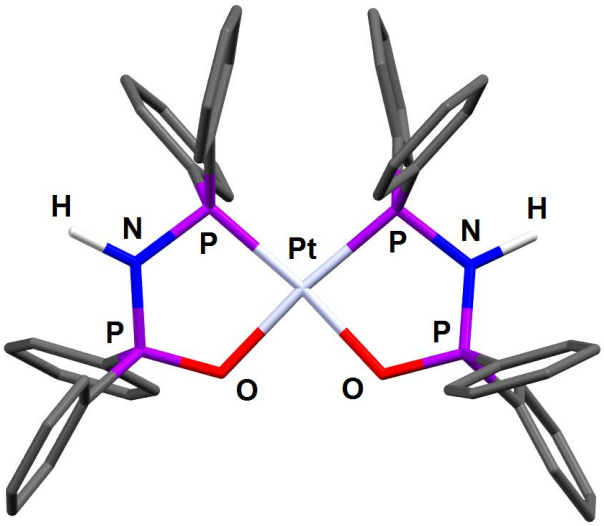

Figure 2. Solid-state structure of the complex *cis*-[Pt{(**DPPA-O**)-*P*,*O*}$_2$][BF$_4$]$_2$ (**13**). The BF$_4$ anions are omitted and only the N-*H* hydrogens are represented for clarity [33].

Woolins and co-workers further studied the reactivity of the complex *cis*-[PtCl$_2${(**DPPA-O**)-*P*}$_2$] (**7**), which once refluxed in MeOH for *ca*. 11 h led to N-PPh$_2$ bond cleavage of one of the **DPPA-O** ligands and formation of *cis*-[PtCl$_2${(**DPPA-O**)-*P*}(PPh$_2$OMe)] (**15**, Scheme 6) [46]. The characteristic ^{31}P NMR data (of the **DPPA-O** ligand) of **15** were found very similar to its *cis*-[PtCl$_2${(**DPPA-O**)-*P*}$_2$] (**7**) precursor (Table 1).

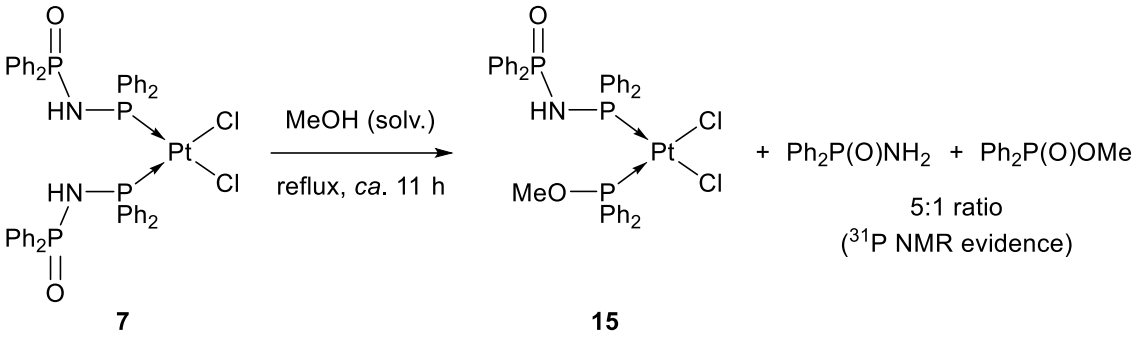

Scheme 6. N-PPh$_2$ bond cleavage of **DPPA-O** in **7** [46].

The formation of complex **15** resulted from a rather unusual/unexpected reactivity, and afforded several by-products, therefore the authors developed a more rational and general route to access Pt^{II} complexes with mixed P-based ligands, through a bridge cleavage of the [PtCl(μ-Cl)(PMe$_2$Ph)]$_2$ dimeric precursor with 2 eq. of **DPPA-O** (Scheme 7) [46]. The latter reaction afforded exclusively the *trans*-[PtCl$_2${(**DPPA-O**)-*P*}(PMe$_2$Ph)] complex (**16**-*trans*), which exhibited in its ^{31}P NMR spectrum a PPh$_2$ resonance significantly downfield shifted compared to a related bis-**DPPA-O** complex, *i.e*. *trans*-[PtI$_2${(**DPPA-O**)-*P*}$_2$] (**9**-*trans*), of *ca*. 7 ppm (Table 1), and accompanied by a typical and very large

$^2J_{P,PMe2Ph}$ coupling constant of 522 Hz. This difference is due to the stronger basicity of the *trans* PMe_2Ph ligand, compared to the PPh_2 moiety of **DPPA-O**. The authors evidenced that the presence of a catalytic amount of **DPPA-O** ligand cleanly and quantitatively isomerizes complex **16**-*trans* into **16**-*cis*, as evidenced by ^{31}P NMR by; 1) an upfield shift of the PPh_2 signal in the same region than other *cis*-[$PtCl_2$(*P*,*P*)] complexes (see *e.g.* **7**, **8**, **15**, Table 1), and 2) a much lower value for the $^2J_{P,PMe2Ph}$ coupling constant (18 Hz). In both complexes (**16**-*trans* and **16**-*cis*), the dangling P=O moiety resonates in the same region as **7**-**11**, **15** and free **DPPA-O** (Table 1). The structure of complex **16**-*cis*, established in the solid-state by XRD analysis, confirmed a slightly distorted square-planar geometry around the Pt^{II} center, with the most obtuse angle being $P_{\mathbf{DPPA\text{-}O}}$-Pt-$P_{Me2Ph}$ [97.62(6)°], probably due to steric factors. The structural parameter (bond lengths and angles) involving the **DPPA-O** ligand are very close to those measured in the related *cis*-[$PtCl_2${(**DPPA-O**)-*P*}$_2$] complex (**7**, Table 1).

Similarly to complexes **1** (Scheme 3), **4** or **7** (Scheme 5), the formation of the *P*,*O*-chelate complexes **17**-*trans* and **17**-*cis* from their respective chloride precursor (**16**-*trans* and **16**-*cis*) was achieved by a chloride abstraction reaction, using a stoichiometric amount of $AgBF_4$ (Scheme 7). The coordination of the P=O moiety was clearly evidenced by ^{31}P NMR spectroscopy, by a significant downfield shift of its resonance (Table 1). The retention of configuration *trans vs*. *cis* was nicely illustrated, by the values of the different P,P and P,Pt coupling constants, and in particular by comparing the $^2J_{P,PMe2Ph}$ of 475 Hz and 13 Hz measured in the *trans* and *cis* isomers, respectively [46].

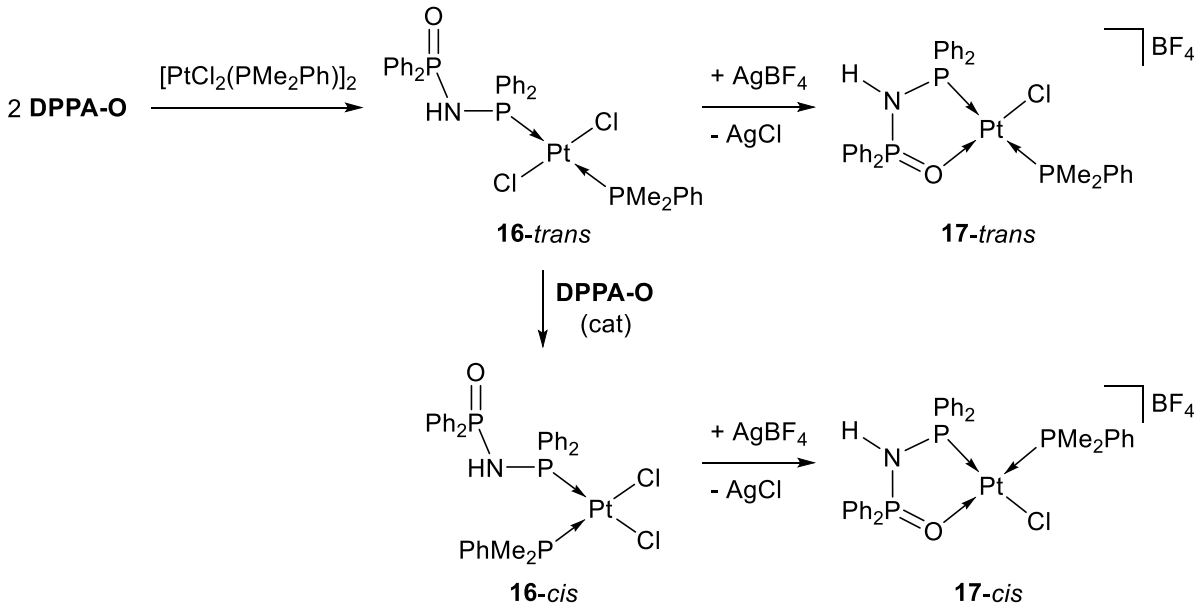

Scheme 7. Synthesis of neutral (**16**) and cationic (**17**) mixed P-based ligands platinum(II) complexes [46].

A series of *C*,*N*-cyclometallated Pd^{II} chloride complexes with monodentate *P*-coordinated **DPPA-O**, of general formula [PdCl(*C*,*N*){(**DPPA-O**)-*P*}] (**18**-**22**, Scheme 8), resulted from the bond cleavage of [Pd(μ-Cl)(*C*,*N*)]$_2$ with 2 eq. of **DPPA-O** [47, 48]. The ^{31}P NMR spectra of complexes **18**-**22** exhibit the expected two doublets (AX spin system) for the two inequivalent P^{III} and P^{V} nuclei. While the resonance assigned to the coordinated PPh_2 moiety is downfield shifted of *ca*. 38-45 ppm relative to the free ligand, the *P*=O group resonates at chemical shift close to that of free **DPPA-O**, indicating no interaction with the metal center (Table 1). Interestingly, when the ^{31}P NMR spectrum of complex **18** was recorded in MeOH (C_6D_6 insert), the resonance of the *P*=O moiety was significantly downfield shifted (from 21.1 to 50.5 ppm) along with a reduction of the $^2J_{P,P=O}$ coupling constant (from 33 to 22 Hz, Table 1). Both observations led the authors to hypothesize that in a methanolic solution the P=O group interact with the metal center, probably *via* the decoordination of the chloride ligand and the formation of a cationic complex. Fliedel and Braunstein and co-workers more recently demonstrated such reactivity in the case of nickel(II) complexes of mono-sulfide *N*-functionalized DPPA-type ligands (see section 5.1).

Complexes **18** and **20** could readily be converted into their cationic *P*,*O*-chelate [Pd(*C*,*N*){(**DPPA-O**)-*P*,*O*}][BF_4] (**23**-**24**) derivatives *via* chloride abstraction with $AgBF_4$ (Scheme 8). As it was observed for the "Pd(ally)" complex **2**, the *P*,*O*-chelation was accompanied by a significant downfield shift of the *P*=O resonances (Table 1). The formation of the *P*,*O*-chelate and the mutual arrangement of the ligands, *i.e*. P *trans* to N and O *trans* to C, were confirmed by single-crystal XRD studies for complex **23** (Figure 3). The coordination angles around the metal are in the range 84.4(3)-96.3(2)°, highlighting a slightly distorted Pd^{II} center. The P-Pd and O-Pd bond lengths are respectively 0.057 Å shorter and 0.048 Å longer than those measured in the "Pd(allyl)" analog complex **2** (Table 1).

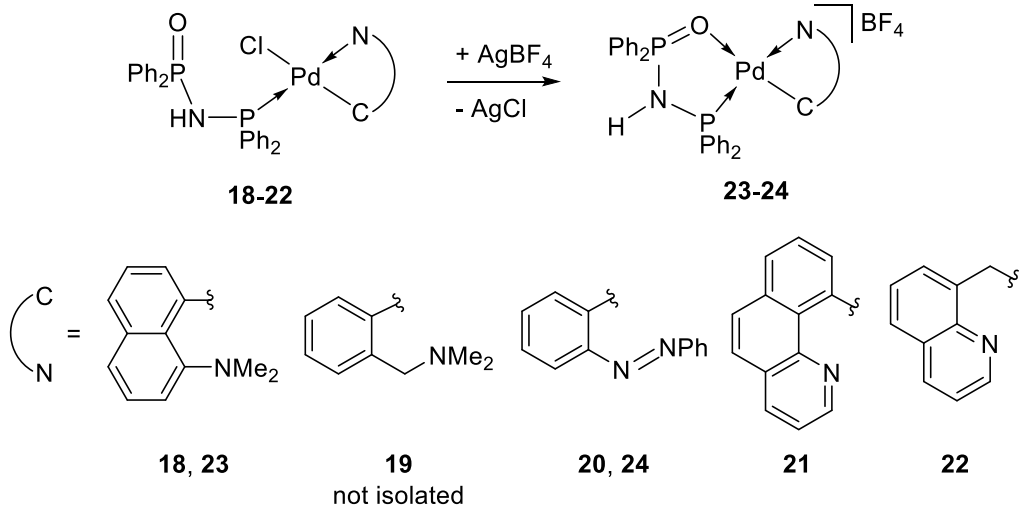

Scheme 8. Synthesis of neutral and cationic *C*,*N*-cyclometallated Pd^{II} complexes of **DPPA-O** [47, 48].

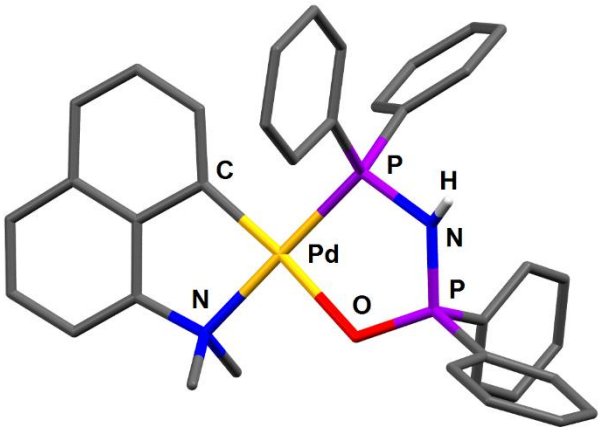

Figure 3. Solid-state structure of the complex [Pd{($C_{12}H_{12}N$)-*C*,*N*}{(**DPPA-O**)-*P*,*O*}][BF_4] (**23**). The BF_4 anion is omitted and only the N-*H* hydrogen is represented for clarity [47].

The stoichiometric reaction between [Pd(CH_3)Cl(COD)] and **DPPA-O** led to the unique example of neutral *P*,*O*-chelate **DPPA-O** Group 10 metal complex [Pd(CH_3)Cl{(**DPPA-O**)-*P*,*O*}] (**25**) *via* substitution of the labile COD ligand (Scheme 9) [49]. The ^{31}P NMR spectrum of complex **25** exhibited the two expected doublets, centered at 65.8 and 44.5 ppm,, while a characteristic N-*H* resonance at δ 8.73 ppm (d_6-DMSO) and an NH absorption band at ν 2988 cm^{-1} could be observed by ^{1}H NMR and FT-IR spectroscopic techniques, respectively (Table 1). The solid-state structure of complex **25**, determined by XRD analysis, revealed a nearly square-planar arrangement of the ligands around the Pd^{II} metal center, with coordination angles in the range 86.93(6)-93.63(6)°. While the P-N (av) and P=O bond lengths and the PNP and OPdP bond angles were found very similar to those measured in the related *P*,*O*- and *C*,*N*-bis-chelate Pd^{II} complex (**23**), the P-Pd and (P=)O-Pd bond lengths in **25** are significantly different by 0.038 and 0.077 Å, respectively.

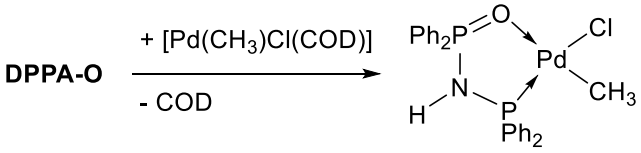

25

Scheme 9. Synthesis of the neutral *P*,*O*-chelate **DPPA-O** Pd^{II} complex (**25**) [49].

Table 1. ^{31}P NMR data and characteristic structural parameters of free **DPPA-O** and Group 10 metal (+2 oxidation state) complexes **1**-**25**.[a]

	M^{II}	$\delta(P^{III})$[b]	$\delta(P^{V})$[b]	$^{2}J_{P,P=O}$	$^{1}J_{P,M}$	$^{2\text{ or }3}J_{P=O,M}$	P=O	P-N[c]	P-M	O-M	PNP	OMP	Ref.
DPPA-O		28.1[d]	21.3[d]	62									[32]
DPPA-O		27.8[e]	25.2[e]	59			1.508(2)	1.679			125.6(2)		[33]
1	Pd	60.9[e]	22.6[e]	37									[32]
2[f]	Pd	59.0[e]	67.8[e]	35			1.496(6)	1.654	2.283(2)	2.103(6)	120.8(4)	86.0(2)	[32]
3	Ni	65.7[g]	71.5[g]	27									[45]
4-*cis*	Pd	58.3[e]	21.1[e]	36[h]									[33]
4-*trans*	Pd	46.7[e]	20.9[e]	25[h]									[33]
5 (*trans*)	Pd	48.5[e]	22.7[e]	22[h]									[33]
6 (*trans*)	Pd	45.4[e]	24.1[e]	23[h]									[33]
7 (*cis*)	Pt	35.7[e]	21.6[e]	22[h]	3955	114	1.481[c]	1.685	2.245[c]	-	131.5[c]	-	[33]
8 (*cis*)	Pt	37.6[e]	22.1[e]	24[h]	3933	104							[33]
9-*cis*	Pt	36.8[e]	21.2[e]	29[h]	3821	108							[33]
9-*trans*	Pt	35.4[e]	22.8[e]	21[h]	2544	83							[33]
10 (*trans*)	Pt	56.0[e]	22.6[e]	18[h]	3202	84	1.472[c]	1.678	2.295[c]	-	131.5[c]	-	[33]
11 (*trans*)	Pt	55.6[e]	23.9[e]	10[h]	3154	88							[33]
12 (*cis*)	Pd	56.3[i]	68.1[i]	6[j]									[33]
13 (*cis*)	Pt	37.4[i]	62.8[i]	3[j]	3924	88	1.502(9)	1.670	2.213(4)	2.108(1)	118.1(7)	87.3(3)	[33]
14 (*cis*)[k]	Pt	58.7[e]	22.7[e]	23[h]	2050								[33]
15 (*cis*)[l]	Pt	36.4[e,m]	22.8[e,m]	26	3963	110							[46]
16-*trans*[l]	Pt	42.7[e,m]	21.6[e,m]	34	2657	79							[46]
16-*cis*[l]	Pt	36.1[e,m]	22.2[e,m]	26	3915	101	1.473(4)	1.673	2.243(1)	-	134.2(3)	-	[46]
17-*trans*[l]	Pt	53.1[e,m]	83.7[e,m]	36	2480	44							[46]
17-*cis*[l]	Pt	46.5[e,m]	68.6[e,m]	9	3383	132							[46]
18[n]	Pd	73.3[e]	21.1[e]	33									[48]
19	Pd	71.7[e]	21.0[e]	33									[48]
20	Pd	69.4[e]	21.9[e]	31									[47]

21	Pd	72.3[e]	21.1[e]	33							[47]
22	Pd	66.4[e]	21.7[e]	35							[48]
23	Pd	73.4[e]	51.5[e]	22	1.512(4)	1.674	2.226(2)	2.151(5)	117.9(3)	87.7(1)	[47, 48]
24	Pd	73.3[e]	53.9[e]	22							[47]
25	Pd	44.5[o]	65.8[o]	23	1.509(2)	1.676	2.188(8)	2.228(2)	117.4(2)	86.93(6)	[49]

[a] Chemical shifts, coupling constants, bond lengths and angles given in ppm, Hz, Å and deg, respectively; [b] appears at doublet unless specified; [c] average value; [d] in C_6D_6/THF; [e] in $CDCl_3$; [f] P^{III} and P^V resonances were not unambiguously attributed; [g] in CD_2Cl_2; [h] $|^2J_{P,P=O} + {}^4J_{P,P'=O}|$; [i] in MeOH/$C_6D_6$; [j] $|^2J_{P,P=O} + {}^{3+4}J_{P,P'=O}|$; [k] in addition to other uncharacterized species; [l] the NMR data reported concern the **DPPA-O** ligand; [m] additional coupling constant(s) involving the monodentate (PPh_2OMe or PMe_2Ph) phosphine ligand are present; [n] $\delta(P^{III}) = 72.2$ ppm, $\delta(P^V) = 50.5$ ppm, $^2J_{P,P=O} = 22$ Hz in MeOH/C_6D_6; [o] in d_6-DMSO, P^{III} and P^V resonances were not assigned.

2.2. Group 9 metal complexes

Within the late transition metals, the development of well-defined rhodium and iridium complexes as (pre)catalysts for various organic transformations represents an attractive field of investigations. Rhodium and iridium species are particularly performant catalysts for the (asymmetric) hydrogenation of unsaturated substrates, such as alkenes or ketones, using molecular hydrogen (H_2) or by H-transfer (typically using an alcohol as H-source) [50-52]. Numerous contributions highlight also the use of Group 9 as efficient tools for C-C, C-O and C-N bond formation *via* C-H bond activation/functionalization [53-55].

Two different Rh^I complexes of **DPPA-O**, of general formula [RhCl(COD){(**DPPA-O**)-*P*}] (**26**) and [RhCl(CO){(**DPPA-O**)-*P*}$_2$] (**31**, Scheme 10), were accessible *via* a bridge cleavage reaction (combined with CO substitution for **31**) of [Rh(μ-Cl)(COD)]$_2$ or [Rh(μ-Cl)(CO)$_2$]$_2$ with 2 or 4 eq. **DPPA-O**, respectively [48]. The ^{31}P NMR spectra of both Rh^I complexes are representative of the expected AMX spin system (^{103}Rh, I = ½, 100% abundance), with the most shifted (to higher frequencies compared to free **DPPA-O**) resonances at *ca*. 61 ppm attributed to the PPh_2 group, while the P=O moiety resonates at a similar chemical shift to that of the free ligand (Table 2). The 1:2 reaction between [Rh(μ-Cl)(CO)$_2$]$_2$ and **DPPA-O** led to a yellow solid, the structure of which was tentatively assigned to [RhCl(CO){(**DPPA-O**)-*P*,*O*}] (**32**), based on ^{31}P NMR data and on the previously reported *cis*-[RhCl(CO){($Ph_2PCH_2P(O)Ph_2$)-*P*,*O*}] complex [56]. The solid-state molecular structure of complex **26** was established by XRD analysis and revealed a slightly distorted square-planar Rh^I center coordinated by the chelating COD ligand, one chlorine and one **DPPA-O** ligand, mono-ligated through the P^{III} donor. While the P=O and P-N (av) bond lengths are similar to those of the free ligand and of most of **DPPA-O** metal complexes, the P-Rh bond length is in the upper range of **DPPA-O** metal complexes. The PNP angle, larger than in the free ligand, is comparable to those measured in the other metal complexes containing monodentate *P*-bonded **DPPA-O** (Table 1 and Table 2).

The Ir^I complex [IrCl(COD){(**DPPA-O**)-*P*}] (**27**) was prepared following the same procedure as its Rh^I analog (**26**, Scheme 10) [48]. The ^{31}P NMR spectra of all Ir^I complexes of **DPPA-O** exhibit two doublet for the non-equivalent P^{III} and P^V nuclei, accounting for a AB spin system, with $^2J_{P,P=O}$ in the range 22-37 Hz (Table 2). As observed for all the metal complexes in which the **DPPA-O** ligand is only *P*-bonded, the resonance of the latter donor in **27** is downfield shifted compared to the free ligand, while the *P*=O resonance is found in the same region.

Similarly to the Group 10 metal complexes (see Section 2.1), the *P*,*O*-chelation of the **DPPA-O** ligand can be favored by halogen abstraction in the Rh^I and Ir^I complexes **26** and **27**, using 1.5 eq. of $AgBF_4$ (Scheme 10) [57]. The corresponding cationic complexes [M(COD){(**DPPA-O**)-*P*,*O*}][BF_4] [M = Rh (**28**), Ir (**29**)] exhibited a significant downfield shift of both P^{III} and P^V resonances in their ^{31}P NMR spectra of *ca*. 17 and 40 ppm, respectively (Table 2). The $^1J_{P,Rh}$ coupling constant remained nearly

unchanged after P=*O* coordination and cationization. Single crystals of complex **28**, analyzed by XRD, revealed a distorted square-planar Rh^{I} metal center, bis-chelated by one COD and one **DPPA-O** ligands (Figure 4). The characteristic structural parameters of **28**, *i.e.* P=O, P-N, P-Rh and O-Rh bond length and PNP and OMP angles are very close to those of the [Pd(allyl)(*P*,*O*)][BF_4] complex **2** (Table 1 and Table 2).

Oxidative-addition reactions are the key step of several catalytic processes. For instance, the Rh-catalyzed methanol carbonylation initially involves the oxidative-addition of MeI to [RhI(CO)(*P*,*P*)] species [58]. Therefore, the study of reaction mechanisms, kinetics and the preparation of model intermediates have attracted much attention [59]. In this context, the reaction of the Ir^{I} complex **29** with MeI afforded the Ir^{III} complex [Ir(Me)I(COD){(**DPPA-O**)-*P*,*O*}][BF_4] (**30**) (Scheme 10). The ^{31}P NMR resonances of the P^{III} and P^{V} nuclei in **30** were found upfield shifted by *ca*. 8 and 37 ppm, respectively, relative to its Ir^{I} parent complex **29**. A typical resonance for the Ir-CH_3 group, which appeared as doublet due to a $^{3}J_{P,H}$ coupling constant of 5 Hz, was observed by ^{1}H NMR spectroscopy. The authors proposed a *cis*-arrangement of the Me and I ligands in complex **30** as depicted in Scheme 10.

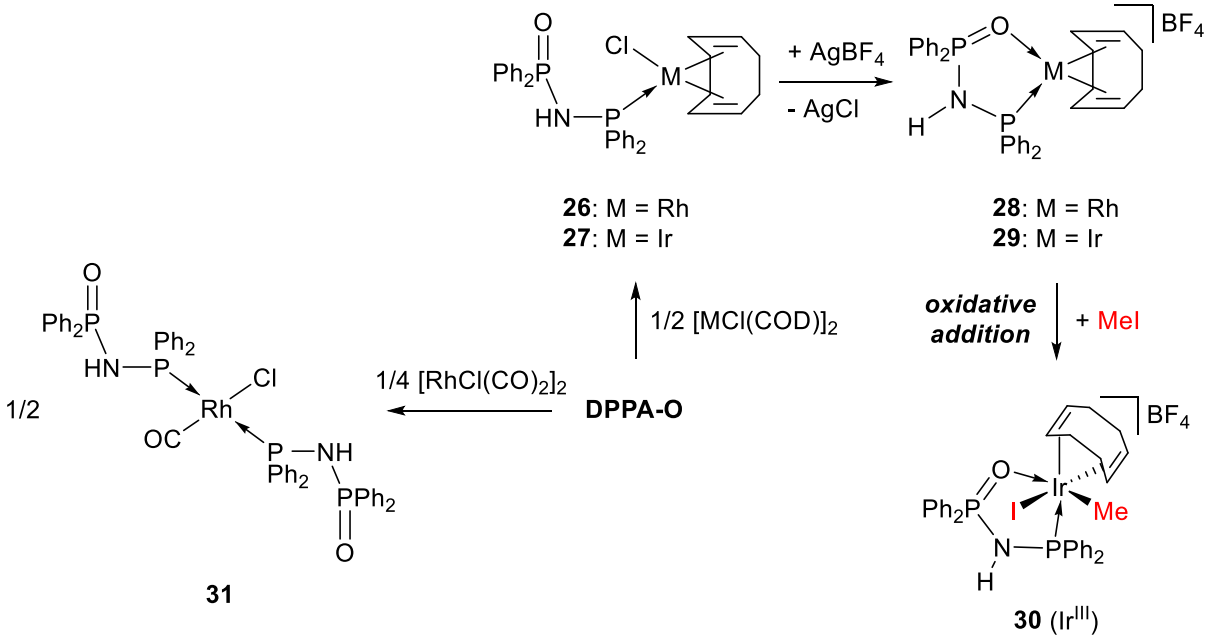

Scheme 10. Synthesis of Rh^{I} and Ir^{I} complexes of **DPPA-O** and reactivity [48, 57].

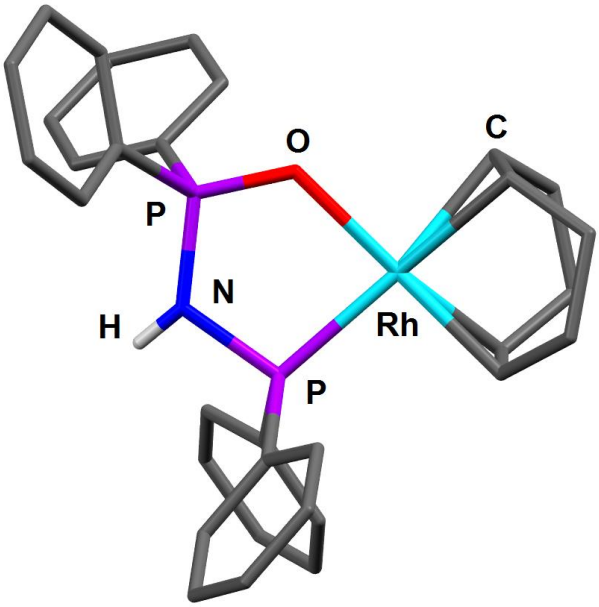

Figure 4. Solid-state structure of the complex [Rh(COD){(**DPPA-O**)-*P*,*O*}][BF_4] (**28**). The BF_4 anion is omitted and only the N-*H* hydrogen is represented for clarity [57].

Woolins and co-workers extended to Rh^{III} and Ir^{III} precursors the strategy that they previously applied to the synthesis of $P_{\mathbf{DPPA\text{-}O}}$-bonded neutral (**26** and **27**) and *P*,*O*-chelate cationic (**28** and **29**) Rh^{I} and Ir^{I} complexes [57]. Chlorido-bridge cleavage of [Cp*MCl(μ-Cl)]$_2$ (M = Rh and Ir) dimeric precursors with 2 eq. **DPPA-O** led to the corresponding neutral [Cp*MCl_2{(**DPPA-O**)-*P*}] [M = Rh (**33**) and Ir (**34**)] complexes, in which the **DPPA-O** ligand is coordinated in a *P*-monodentate mode (Scheme 11). Chloride abstraction from the latter, using $AgBF_4$, led to the corresponding cationic *P*,*O*-chelate [Cp*MCl{(**DPPA-O**)-*P*,*O*}][BF_4] [M = Rh (**35**) and Ir (**36**)] complexes (Scheme 11). The ^{31}P NMR data of the "Cp*M^{III}" complexes **33**-**34** and **35**-**36** are very similar, both in shapes and chemical shifts, to those of their "M^{I}(COD)" derivatives (**26**-**27** and **28**-**29**, respectively, Table 2).

In the different Group 9 metal complexes of **DPPA-O** presented in this section, the neutral nature of the ligand could be assessed by the observation of a ν(N-H) absorption band in the 3163-3244 cm^{-1} region in their respective FT-IR spectra [48, 57].

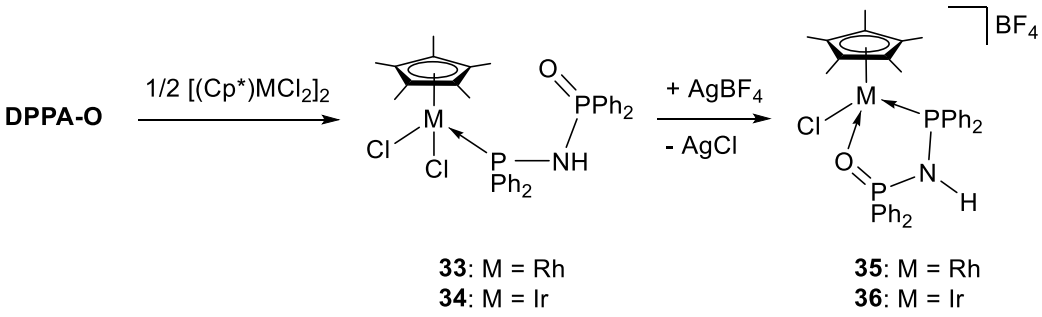

33: M = Rh
34: M = Ir

35: M = Rh
36: M = Ir

Scheme 11. Synthesis of Rh^{III} and Ir^{III} complexes of **DPPA-O** [57].

Table 2. ^{31}P NMR data and characteristic structural parameters of free **DPPA-O** and Group 9 metal complexes **26**-**36**.[a]

	M	$\delta(P^{III})$[b]	$\delta(P^{V})$[b]	$^{2}J_{P,P=O}$	$^{1}J_{P,M}$	$^{2\text{ or }3}J_{P=O,M}$	P=O	P-N[c]	P-M	O-M	PNP	OMP	Ref.
DPPA-O		28.1(d)[d]	21.3(d)[d]	62									[32]
DPPA-O		27.8(d)[e]	25.2(d)[e]	59			1.508(2)	1.679			125.6(2)		[33]
26	Rh^{I}	60.4 (dd)[e]	21.3 (dd)[e]	40	159	5	1.478(4)	1.687	2.289(1)		132.6(3)		[48]
27	Ir^{I}	49.2 (d)[e]	22.6 (d)[e]	35									[48]
28	Rh^{I}	75.6 (dd)[e]	61.5 (d)[e]	35	154		1.507(4)	1.674	2.272(2)	2.092(4)	119.0(3)	85.9(1)	[57]
29	Ir^{I}	69.6 (d)[e]	65.5 (d)[e]	31									[57]
30	Ir^{III}	61.7 (d)[e]	28.2 (d)[e]	22									[57]
31	Rh^{I}	62.4 (dd)[e]	20.8 (dd)[e]	26	127	3							[48]
32	Rh^{I}	86.6 (dd)[f]	54.7 (d)[f]	32	161								[48]
33	Rh^{III}	66.2 (dd)[e]	21.1 (dd)[e]	41	147	4							[57]
34	Ir^{III}	35.7 (d)[e]	21.1 (d)[e]	37									[57]
35	Rh^{III}	76.5 (dd)[e]	58.0 (d)[e]	25	147								[57]
36	Ir^{III}	65.9 (d)[e]	58.4 (d)[e]										[57]

[a] Chemical shifts, coupling constants, bond lengths and angles given in ppm, Hz, Å and deg, respectively; [b] multiplicity of the NMR signals given in parenthesis; [c] average value; [d] in C_6D_6/THF; [e] in $CDCl_3$; [f] in DMSO/C_6D_6.

2.3. Group 8 metal complexes

Group 8 metal complexes are attractive species due to their wide range of catalytic applications, which embrace for example C-H bond functionalization, C-C coupling and (asymmetric) hydrogenation or silylation [53, 60-64]. Within the Group 8 metals, the development of well-defined iron catalysts is attracting increasing attention due to its high abundance, low cost, and relatively low toxicity [65-67].

Smith and Woolins and co-workers reported the synthesis of two series of Ru^{II}, Os^{II} and Ru^{IV} complexes of **DPPA-O** [57, 68]. The first group of neutral complexes [(L)MCl_2{(**DPPA-O**)-*P*}] [L = *p*-Cym, M = Ru (**37**) and Os (**38**); L = η^3: η^3-$C_{10}H_{16}$, M = Ru (**39**)], in which the mixed *P*,P=*O* is coordinated in a monodentate mode by the P^{III} donor, are readily obtained by bridge cleavage reaction of their corresponding chlorido-bridged dimeric precursors, [(L)M$Cl(\mu$-Cl)] [L = *p*-Cym, M = Ru or Os; L = η^3: η^3-$C_{10}H_{16}$, M = Ru], with 2 eq. **DPPA-O** ligand (Scheme 12). This first set of compounds can be ionized by chloride abstraction with $AgBF_4$, affording their cationic [(L)MCl{(**DPPA-O**)-*P*,*O*}][BF_4] [L = *p*-Cym, M = Ru (**40**) and Os (**41**); L = η^3: η^3-$C_{10}H_{16}$, M = Ru (**42**)] derivatives, in which the **DPPA-O** ligand is *P*,*O*-chelating (Scheme 12).

The ^{31}P NMR signal of the *P*Ph_2 group of the **DPPA-O** ligand was subject to a significant downfield shift (*ca*. 32 ppm) upon coordination to Ru in **37** and **39** (Table 3). In contrast, the *P*=O resonance was not much affected in the latter, and was found in the same range than for the free ligand. Similar observations were made for the Group 9 and 10 metal complexes supported by the **DPPA-O** ligand in a monodentate *P*-coordination mode (see Sections 2.1 and 2.2). Interestingly, the Os^{II} complex **38** did not exhibit a similar behavior: while the *P*=O resonance remained in the expected region for the non-coordinated P=O moiety (*ca*. 20 ppm), the *P*Ph_2 resonance was slightly upfield shifted to a similar chemical shift (Table 3). Upon cationization and *P*,*O*-chelation, both *P*Ph_2 and *P*=O ^{31}P NMR resonances of complexes **40**-**42** were significantly downfield shifted compared to their neutral parent complexes (**37**-**39**), especially the *P*=O group which shifted from the "non-coordinated" region(*ca*. 20 ppm) to 51-66 ppm (Table 3). No deprotonation of the N-*H* moiety was observed, as assessed by the presence of the characteristic *ν*(N-H) absorption band in the 3132-3253 cm^{-1} region in the FT-IR spectra of complexes **37**-**42** [57, 68].

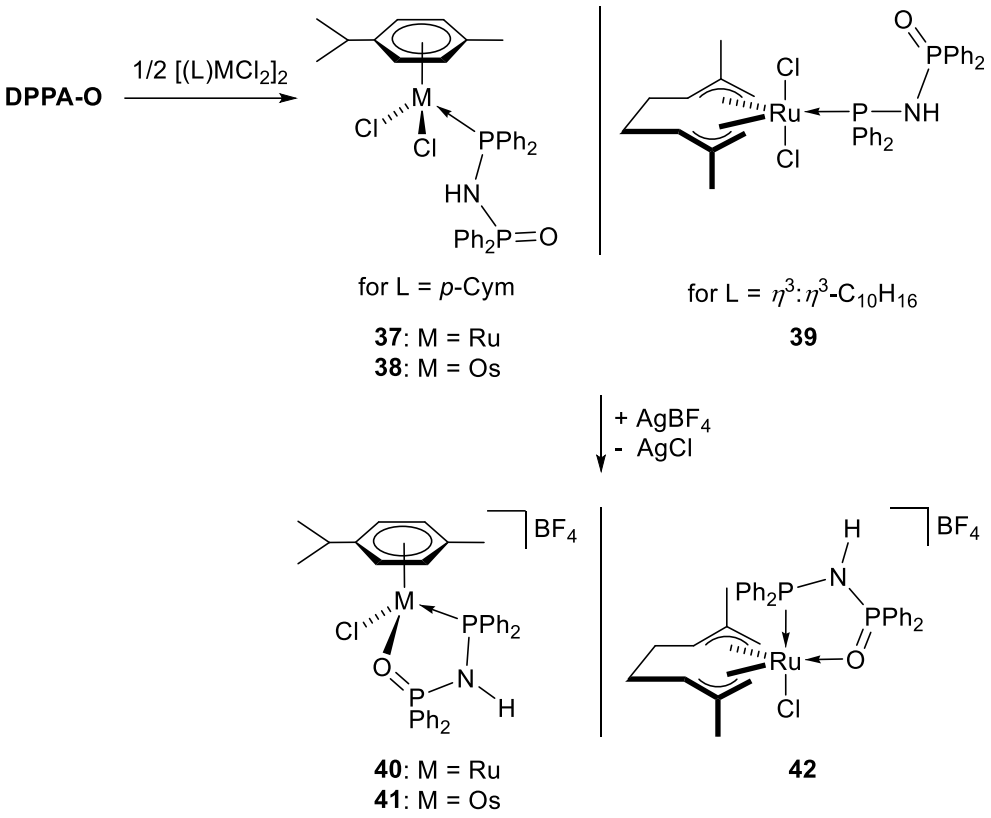

Scheme 12. Synthesis of Ru^{II}, Os^{II} and Ru^{IV} metal complexes of **DPPA-O** [57, 68].

The solid-state structures of the Os^{II} complexes **38** and **41**, established by XRD analysis, featured in both cases a distorted tetrahedral piano-stool geometry around the metal center. Invariant parameters of the Os^{II} coordination sphere are the presence of one *p*-Cym ligand (η^6-coordination mode) and one chlorine ligand, while the two other coordination sites are occupied by: 1) one chlorine and one *P*-monodentate bonded **DPPA-O** ligand in **38** or 2) one *P*,*O*-chelating **DPPA-O** ligand in **41** (Figure 5). The P=O, P-N and P-Os bond lengths are very close in the two compounds and in the same range than those measured in the Rh^{I} complexes **26** and **28** (Table 3 *vs*. Table 2). The transition of monodentate *P*- to bidentate *P*,*O*-chelating mode of the **DPPA-O** ligand induces a lowering of the PNP angle value from *ca*. 130 to 120°, as observed in analogous Group 9 and 10 metal complexes (see Table 1-Table 3).

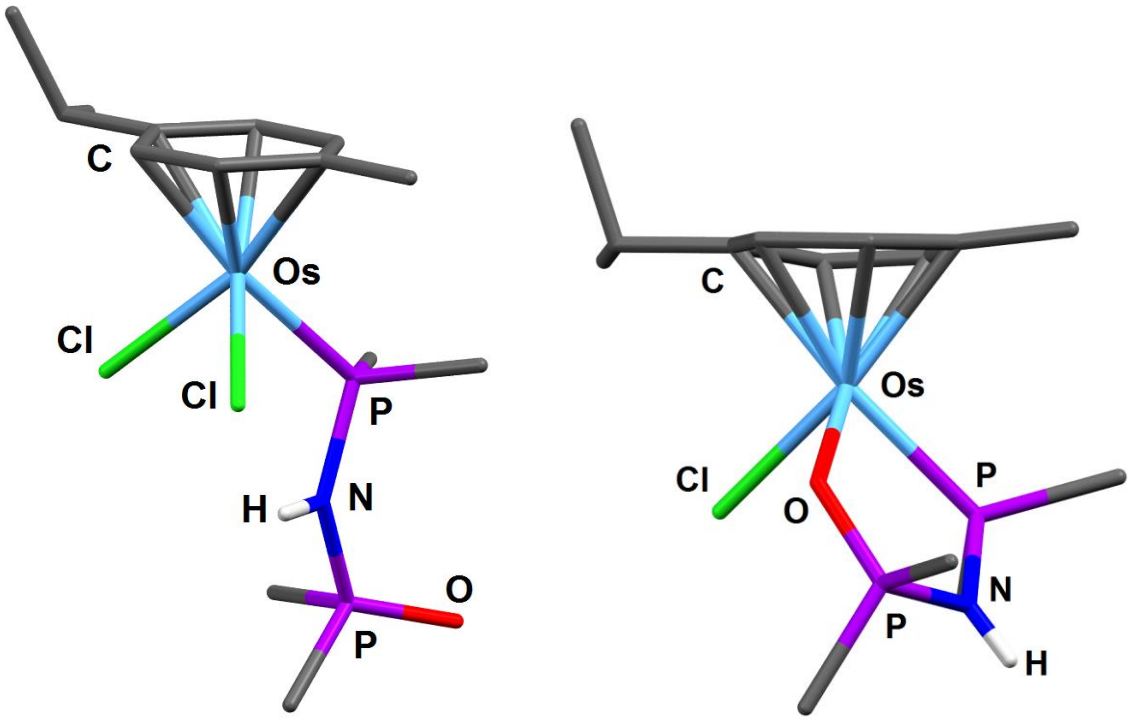

Figure 5. Solid-state structures of the [(*p*-Cym)$OsCl_2${(**DPPA-O**)-*P*}] (**38**, left) and [(*p*-Cym)OsCl{(**DPPA-O**)-*P*,*O*}][BF_4] (**41**, right) complexes. The BF_4 anion (in **41**) is omitted and only the N-*H* hydrogen and *ipso*-C of the P*Ph* rings are represented for clarity [68].

Table 3. ^{31}P NMR data and characteristic structural parameters of free **DPPA-O** and Group 8 metal complexes **37**-**42**.[a]

	M	$\delta(P^{III})^b$	$\delta(P^{V})^b$	$^2J_{P,P=O}$	P=O	P-N[c]	P-M	O-M	PNP	OMP	Ref.
DPPA-O		28.1[d]	21.3[d]	62							[32]
DPPA-O		27.8[e]	25.2[e]	59	1.508(2)	1.679			125.6(2)		[33]
37	Ru^{II}	62.1[e]	20.4[e]	40							[57]
38	Os^{II}	20.6[e,f,g]	20.3[e,f,g]	[f]	1.479[h]	1.677[h]	2.342[h]		129.6[h]		[68]
39	Ru^{IV}	58.5[e]	19.6[e]	44							[57]
40	Ru^{II}	82.1[e,g]	65.0[e,g]	29							[57]
41	Os^{II}	70.2[e]	51.3[e]	26	1.514[h]	1.677[h]	2.318[h]	2.139[h]	119.9[h]	83.5[h]	[68]
42	Ru^{IV}	66.5[e]	65.8[e]	34							[57]

[a] Chemical shifts, coupling constants, bond lengths and angles given in ppm, Hz, Å and deg, respectively; [b] appears at doublet unless specified; [c] average value; [d] in C_6D_6/THF; [e] in $CDCl_3$; [f] $^2J_{P,P=O}$ is not observed, resulting in singlet resonances for both P^{III} and P^{V} nuclei; [g] P^{III} and P^{V} resonances were not assigned by the authors; [h] average value due to the presence of two molecules in the asymmetric unit.

2.4. Other metal complexes

Rossi *et al*. reported the formation of the neutral rhenium(III) [$ReCl_3(H_2O)$\{(**DPPA-O**)-*P*,*O*\}] (**43**) or rhenium(IV) [$ReCl_4$\{(**DPPA-O**)-*P*,*O*\}] (**44**) complexes of **DPPA-O**, by reaction between the anionic rhenium(V)-oxo precursor [$AsPh_4$][$ReOCl_4$] and (non-oxidized) **DPPA** in a 1:1 molar ratio, depending on the reaction conditions (Scheme 13) [69]. The formation of the $ReCl_4$ complex (**44**), rather than the aquo complex (**43**), is triggered by the use of anhydrous chloroform as solvent, all other synthetic parameters being equal. More interestingly is the "oxo-shift" from the rhenium precursor to the ligand, leading to an *in-situ* oxidation of **DPPA** (two P^{III} atoms) to **DPPA-O** (mixed P^{III}/P^{V} atoms) and reduction of Re^{V} to Re^{III}. However, the authors do not discuss the different changes in oxidation states. Both complexes **43** and **44** are paramagnetic species in the solid-state, exhibiting a magnetic moment of 2.80 and 3.2 μ_B at 27°C, respectively. In their FT-IR spectra the characteristic *v*(N-H) absorption band was observed in the 2617-2546 cm^{-1} region. The slightly distorted octahedral coordination geometry around the Re metal centers and the *P*,*O*-chelating mode of the **DPPA-O** ligands in **43**-**44** were confirmed in the solid-state by XRD analysis. In **43**, the water molecule was found *trans* to the P=*O* ligand. The structural parameters, *i.e*. bond lengths and angles, of complexes **43**-**44** are very close to each other (Table 4). However, the P-Re bond is longer and the (P=)O-Re bond is shorter than those measured in all other structurally characterized metal complexes of **DPPA-O** (see Table 1-Table 3).

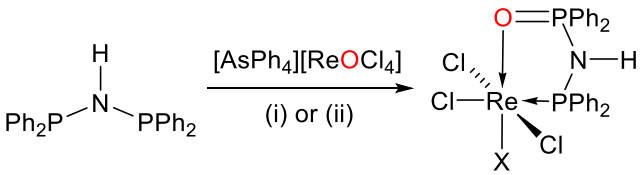

DPPA

43: (i) X = H_2O
44: (ii) X = Cl

Scheme 13. Synthesis of Re^{III} (**43**) and Re^{IV} (**43**) complexes of **DPPA-O** starting from a Re^{V}-oxo precursor and non-oxidized **DPPA**. Conditions: (i) degassed $CHCl_3$, reflux, 30 min; (ii) anhydrous degassed $CHCl_3$, reflux, 30 min [69].

Stoichiometric reaction between [AuCl(THT)] and **DPPA-O** led to the substitution of the labile THT ligand and formation of the [AuCl{(**DPPA-O**)-*P*}] complex **45**, in which the mixed P/P=O ligand is mono-ligated through the P^{III} donor (Scheme 14) [48]. The ^{31}P NMR spectrum of complex **45** exhibited two singlets ($J_{P,P=O}$ not resolved) at δ 53.9 and 26.4 ppm, attributed to the coordinated *P*Ph_2 and free *P*=O groups, respectively (Table 4). A characteristic *v*(N-H) absorption band at 3009 cm^{-1} was also observed by FT-IR spectroscopy for this two-coordinated Au^{I} complex.

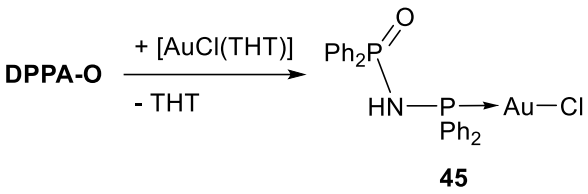

45

Scheme 14. Synthesis of the gold(I) chloride complex (**45**) of **DPPA-O** [48].

Table 4. ^{31}P NMR data and characteristic structural parameters of free **DPPA-O** and metal complexes **43**-**45**.[a]

	M	$\delta(P^{III})^b$	$\delta(P^{V})^b$	$^2J_{P,P=O}$	P=O	P-N[c]	P-M	O-M	PNP	OMP	Ref.
DPPA-O		28.1[d]	21.3[d]	62							[32]
DPPA-O		27.8[e]	25.2[e]	59	1.508(2)	1.679			125.6(2)		[33]
43	Re^{III}				1.522(1)	1.665	2.468(4)	2.055(9)	119.3(6)	80.9(4)	[69]
44	Re^{IV}				1.512[f]	1.668[f]	2.499[f]	2.068[f]	118.8[f]	79.6[f]	[69]
45	Au^{I}	53.9[e]	26.4[e]	[g]							[48]

[a] Chemical shifts, coupling constants, bond lengths and angles given in ppm, Hz, Å and deg, respectively; [b] appears at doublet unless specified; [c] average value; [d] in C_6D_6/THF; [e] in $CDCl_3$; [f] average value due to the presence of two molecules in the asymmetric unit; [g] not resolved.

3. *N*-substituted mono-oxide DPPA-type ligands

Woolins and co-workers reported the derivation of a chiral diphosphine (DPPA-type) ligand, based on the (*S*)-alanine methyl ester scaffold, by oxidation of one (or two) P atom(s) with H_2O_2 [70]. Unfortunately, the targeted mono-oxide *N*-substituted DPPA-type ligand **46** was found unstable in solution and transforms into the bis-oxide derivative, however its ^{31}P NMR fingerprint could be recorded [δ 45.8 (d, *P*Ph_2), 33.2 (d, *P*=O) ppm; $^2J_{P,P=O}$ 80 Hz]. Interestingly, the mixed P^{III}/P^{V} ligand **46** could be generated *in-situ* and further reacted with 1/3-1/2 eq. (depending on the purity determined by ^{31}P NMR) of the [$PdCl_2$(COD)] precursor to form the [$PdCl_2${(**46**)-*P*,*O*}] complex **47** (Scheme 15). The ^{31}P NMR spectrum of complex **47** exhibited the expected AX spin system composed of two doublets centered at 78.6 and 61.7 ppm ($^2J_{P,P=O}$ 34 Hz), for the non-equivalent P^{III} and P^{V} nuclei, respectively. Although they are markedly different, the cationic Pd^{II} complexes of the *P*,*O*-chelating **DPPA-O** ligand (**23**-**24**) exhibit comparable NMR data (Table 1). Furthermore, the solid-state structure of **47**, established by XRD analysis, confirmed a distorted square-planar Pd^{II} center, with coordination angles ranging from 87.8(2) to 93.81(11)°, coordinated by one *P*,*O*-chelating ligand **46** and two chlorine atoms (Figure 6). While the P-Pd [2.214(3) Å] and (P=)O-Pd [2.039(7) Å] bond lengths were slightly shorter, the P=O [1.524(7) Å] and P-N (av. 1.703 Å) bond lengths of complex **47** were slightly longer than those measured in the Pd^{II} complexes of **DPPA-O** (Section 2.1, Table 1). On the other hand, both PNP [115.5(5)°] and OPdP [87.8(2)°] angles were in the same ranges [70].

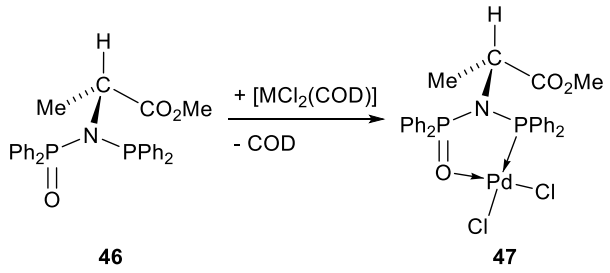

Scheme 15. Synthesis of the palladium(II) chloride complex (**47**) of ligand **46** [70].

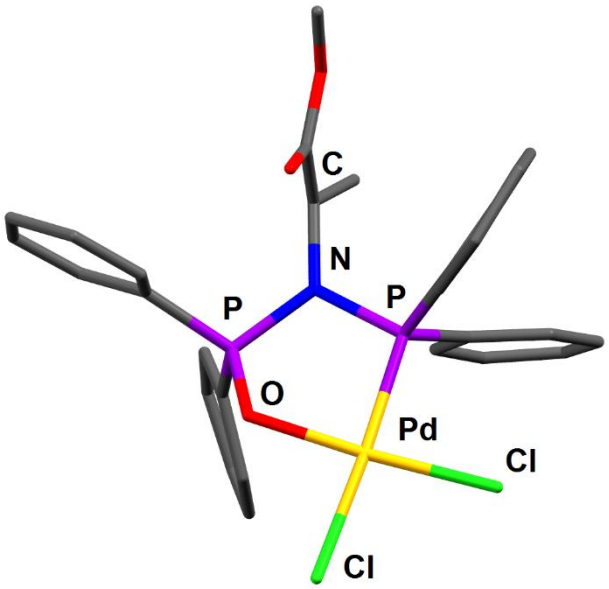

Figure 6. Solid-state structure of the complex [$PdCl_2${(**46**)-*P*,*O*}] (**47**). The H atoms are omitted for clarity [70].

4. DPPA mono-sulfide (**DPPA-S**)

The heteroditopic ligand **DPPA-S** can be readily prepared by reaction between **DPPA** and elemental sulfur (S_8, Scheme 16), however a small amount (≈ 5%) of the bis-sulfide derivative (**DPPA-S_2**) was inevitably formed [71]. The ^{31}P NMR spectrum of **DPPA-S** exhibited the expected two doublets ($^2J_{P,P=S}$ = 86 Hz) for the non-equivalent P^{III} and P^{V}(=S) nuclei (AX spin system), centered at 27.6 and 60.9 ppm, respectively (Table 5). A characteristic absorption band at ν = 3165 cm^{-1}, undeniably attributed to the N-H group stretching mode, is very close to the frequency of same vibration in **DPPA** (ν = 3230 cm^{-1}).

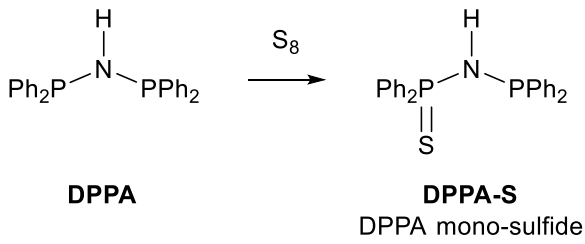

Scheme 16. Synthesis of **DPPA-S** [71].

Reaction between **DPPA-S** and Group 10 metal precursors of the $[MCl_2(L_2)]$ (M = Ni, Pd, Pt; L_2 = DME, COD) type led to different outcomes. The reaction with the Pd^{II} precursor, in a 2:1 ligand/metal ratio, afforded a mixture of both *cis* and *trans* isomers (1:5 ratio) of the expected dicationic complex $[Pd\{(\mathbf{DPPA\text{-}S})\text{-}P,S\}_2][Cl]_2$ (**48**, Scheme 17). In contrast, ligand deprotonation occurred upon coordination with Pt^{II} under similar reaction conditions, forming the neutral complex *cis*/*trans*-$[Pt\{(\mathbf{DPPA\text{-}S_{-H}})\text{-}P,S\}_2]$ [71]. The equimolar reaction between **DPPA-S** and $[NiCl_2(DME)]$ afforded solely the complex *trans*-$[Ni\{(\mathbf{DPPA\text{-}S})\text{-}P,S\}_2][Cl]_2$ (**49**, Scheme 17) and unreacted Ni^{II} precursor [72]. These results strongly contrast with those observed with **DPPA-O** (see section 2.1), which preferably formed $[MCl_2\{(\mathbf{DPPA\text{-}O})\text{-}P\}_2]$ (M = Pd, Pt) complexes, and suggest a much greater preference for **DPPA-S** to form chelates than **DPPA-O**. The ^{31}P NMR spectra of complexes **48** (mixture of both *cis* and *trans* isomers) and **49** exhibited two triplets for the magnetically non-equivalent P^{III} and P^{V} nuclei of each bis-chelate complex, significantly downfield shifted compared to the free ligand (Table 5). A complex AA'BB' spin system, involving $^{2+3}J_{P,P=S} = {}^{2+3}J_{P',P'=S}$, $^{3+4}J_{P,P'=S}$, $^{4}J_{P=S,P'=S}$, $^{2}J_{P,P'}$, could be evidenced and successfully simulated for the Ni^{II} complex **49**. Moreover, the solid-state molecular (centrosymmetric) structure of the latter, determined by XRD analysis, confirmed the formation of a tetra-coordinate dicationic Ni^{II} center, bis-chelated by two **DPPA-S** ligands, *trans* to each other (Figure 7). Both P-Ni and S-Ni bond lengths are very close, and the P-Ni-S angle approaches 90°, which resulted in a very weak distortion from ideal square-planar geometry. The latter geometry resulted in the formation of a diamagnetic Ni^{II} complex. The P=S bond length of 2.0281(15) Å is somewhat longer than the P=O bond in Group 10 metal complexes of **DPPA-O** (range: 1.472-1.512 Å, Table 1). The dicationic charge of the metal complex is balanced by two chlorides, which exhibit H-bonding interactions with the N-*H* atom. Characteristic *v*(N-H) absorption bands at *ca.* 2700 cm^{-1} were recorded in the FT-IR spectra of complexes **48** and **49** [71, 72].

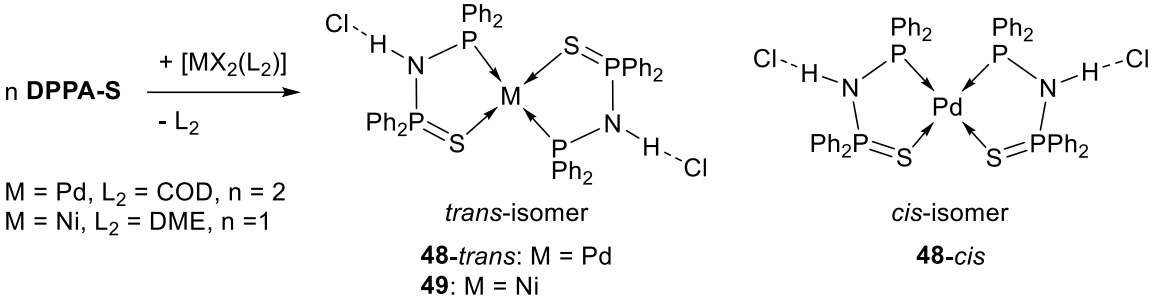

Scheme 17. Synthesis of Group 10 metal complexes of **DPPA-S** [71, 72].

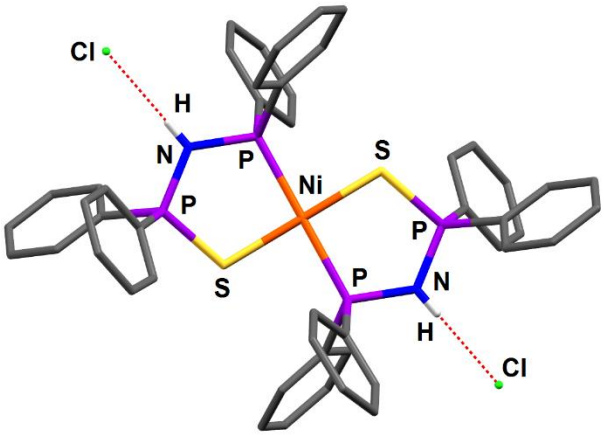

Figure 7. Solid-state structure of the complex [Ni{(**DPPA-S**)-*P*,*S*}$_2$][Cl]$_2$ (**49**). Only the N-*H* hydrogen is represented for clarity [72].

An original approach to piano-stool Group 8 and 9 metal complexes of **DPPA-S**, reported by Valderrama and colleagues, consists in two or three steps [73, 74]. The first step involves a bridge cleavage of [(L)MCl(μ-Cl)]$_2$ (M = Ru, Rh, Ir, L = *p*-Cym, C_6M_6, Cp*) by 2 eq. of **DPPA**, which resulted in the formation of the corresponding [(L)MCl$_2${(**DPPA**)-*P*}] complexes, with **DPPA** acting as a monodentate ligand. Subsequent selective oxidation of the uncoordinated P atom of **DPPA** with elemental sulfur (1 eq.) led to complexes [(L)MCl$_2${(**DPPA-S**)-*P*}] (**50**-**53**, Scheme 18), supported by one **DPPA-S** ligand in a *P*-monodentate coordination mode. The stoichiometric reaction of complexes **50**-**53** with a silver salt led to different results. While the Ir^{III} complex **53** reacted cleanly with $AgBF_4$ to form the *P*,*S*-chelate cationic complex [Cp*IrCl{(**DPPA-S**)-*P*,*S*}][BF_4] (**56**, Scheme 18), under similar reaction conditions the Ru^{II} and Rh^{III} complexes **51**-**52** underwent deprotonation of the acidic N-*H* group and formed the neutral complexes [(L)MCl{(**DPPA-S$_{-H}$**)-*P*,*S*}] [73]. The authors also demonstrated that the Ir^{III} complex **56** could be accessible in a similar yield (63 *vs*. 66 %), by a one-pot reaction between [Cp*IrCl(μ-Cl)]$_2$, isolated **DPPA-S** and $AgBF_4$, in a 1:2:2 molar ratio [73]. In the case of the Ru^{II} complex **50**, the outcome of the reaction was found dependent on the solvent used. When the reaction was performed in EtO_2 the expected cationic *P*,*S*-chelate complex [(C_6Me_6)RuCl{(**DPPA-S**)-*P*,*S*}][BF_4] (**54**, Scheme 18) was isolated. In contrast, the use of CH_2Cl_2 as solvent promoted, as for **51** and **52**, the deprotonation of the **DPPA-S** ligand [74]. The ^{31}P NMR data of complexes **50**-**56** are reported in Table 5. The authors observed a large deshielding of the PPh_2 resonance upon coordination of **DPPA-S** ($\Delta\delta$ = *ca*. +45 ppm) for the neutral Ru^{II} and Rh^{III} complexes (**50**-**52**), while a smaller shift was recorded for the Ir^{III} derivative (**53**), similarly to what was observed for analogous complexes of **DPPA-O** (see sections 2.2 and 2.3, Table 2 and Table 3). In all complexes where the *P*=S moiety remained uncoordinated (**50**-**53**), its characteristic doublet resonance was observed at *ca*. 51 ppm. The formation of the cationic *P*,*S*-chelate species **54**-**56** resulted in downfield shifts of both *P*Ph_2 and *P*=S resonances. The assignment of the P^{III} *vs*. P^{V} resonance was facilitated by the presence of $^1J_{P,Rh}$ couplings in **52** and **55**. Characteristic

v(N-H) absorption bands centered at 3070 and 3330 cm^{-1} were observed in the FT-IR spectra of the Ru^{II} complexes **50** and **54** [74].

An attempt to coordinate the mono-sulfide DPPA-type ligand (*S*)-(PPh_2)N{P(S)Ph_2}(CHMePh) (**59**, section 5) to *in-situ* generated [Cp*MCl(S)$_x$][BF_4] (M = Rh, Ir, S = solvent) yielded complexes **55** and **56**, consequently to the "loss" of the *N*-group [75]. The identity of complexes **55** and **56** was established by NMR and XRD analysis, which confirmed the formation of piano-stool Rh^{III} and Ir^{III} complexes coordinated by one η^5-Cp* ring, one **DPPA-S** ligand in a *P*,*S*-chelating mode, and one chlorine atom, while the cationic charge is balanced by one BF_4 anion (Figure 8). The characteristic bond lengths and angles in both complexes **55** and **56** are very close, and in the same range than those measured in the Ni^{II} complex **49**, with the exception of the P-M and S-M bond lengths, as anticipated for a larger atomic radius for Rh and Ir *vs*. Ni (Table 5).

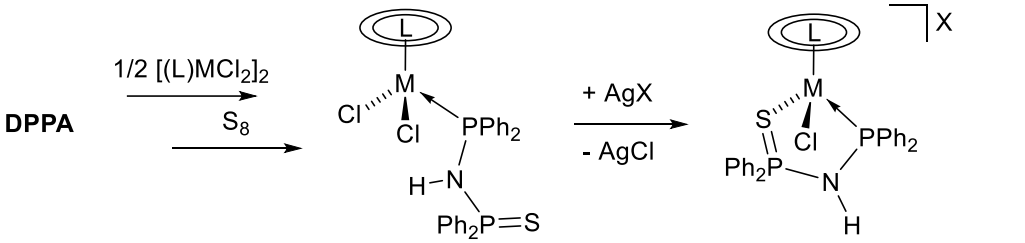

50: M = Ru, L = C_6Me_6
51: M = Ru, L = *p*-Cym
52: M = Rh, L = Cp*
53: M = Ir, L = Cp*

54: M = Ru, L = C_6Me_6, X = PF_6
55: M = Rh, L = Cp*, X = BF_4
56: M = Ir, L = Cp*, X = BF_4

Scheme 18. Synthesis of Group 8 and 9 metal complexes of **DPPA-S** [73, 74]. Note: complex **55** was not obtained *via* this route, see text and ref [75].

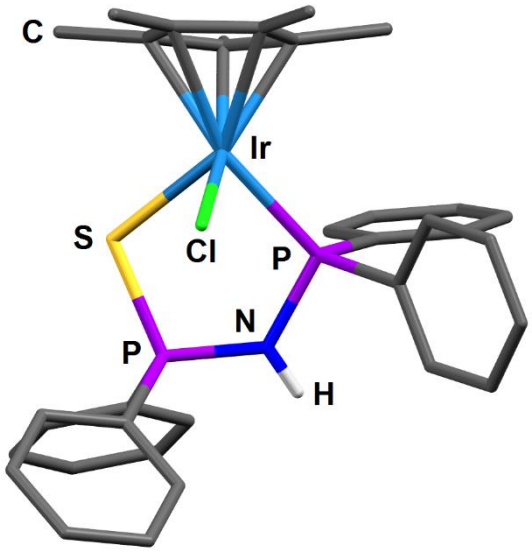

Figure 8. Solid-state structure of the complex [Cp*IrCl{(**DPPA-S**)-*P*,*S*}][BF_4] (**56**). The BF_4 anion is omitted and only the N-*H* hydrogen is represented for clarity [75].

Recently, Tsukuda, Tsubomura and co-workers reported an original copper(I)-mediated sulfur transfer reaction from **DPPM-S$_2$** to other phosphines, including **DPPA**, which led in the latter case to the formation of the heteroleptic bis-chelated cationic Cu^{I} complex [Cu{(**DPPM-S**)-*P*,*S*}{(**DPPA-S**)-*P*,*S*}][PF$_6$] (**57**), which incorporated one **DPPM-S** and one **DPPA-S** ligand (Scheme 19) [76]. The ^{31}P NMR spectrum of **57** exhibited two set of signals for two unsymmetrical diphosphine ligands, *i.e*. **DPPA-S** and **DPPM-S**, which combined with the multiple splitting of the low field signals, confirmed that the proposed structure is retained in solution. The authors proposed a mechanism consisting in an initial coordination of the bis-sulfide **DPPM-S$_2$** ligand to Cu^{I}, which is followed by the coordination of the diphosphine (**DPPA**) in a monodentate mode, allowing subsequent attack of the free P atom to one (coordinated) S atom, to give a P-S-P intermediate. Subsequently, sulfur transfer occurs to give the final complex. Presumably, this sulfur transfer reaction is disfavored when using diphosphine ligands that form more stable chelates (*e.g*. with a propylene or butylene spacer instead of NH), because of the lower availability of the P atom(s) to attack the S.

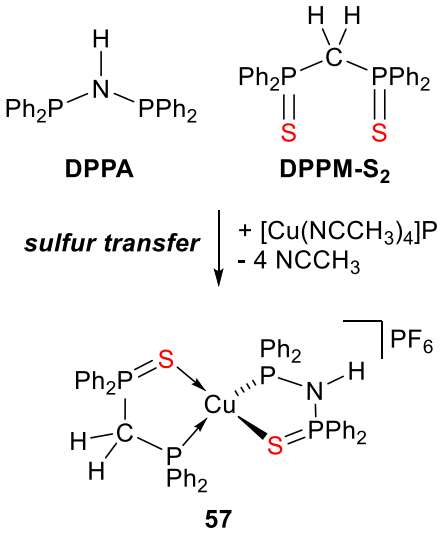

Scheme 19. Cu^{I}-mediated sulfur transfer from **DPPM-S$_2$** to **DPPA** to form the bis-*P*,*S*-chelate complex **57** [76].

Table 5. ^{31}P NMR data and characteristic structural parameters of free **DPPA-S** and metal complexes **48**-**57** (Table divisions: free ligand, Group 10 metals, piano-stool Group 8-9 metal complexes, Group 11 metal).[a]

	M	$\delta(P^{III})$[b]	$\delta(P^{V})$[b]	$^{2}J_{P,P=S}$	P=S	P-N[c]	P-M	S-M	PNP	SMP	Ref.
DPPA-S		27.6(d)[d]	60.9(d)[d]	86							[71]
48-*trans*	Pd^{II}	79.7(t)[e]	76.1(t)[e]	46[f]							[71]
48-*cis*	Pd^{II}	78.2(t)[e]	68.8(t)[e]	20[f]							[71]
49	Ni^{II}	79.2(t)[g]	82.8(t)[g]	64[h]	2.028(2)	1.658	2.205(1)	2.178(1)	121.0(2)	92.0(4)	[72]
50	Ru^{II}	68.0(d)[e]	50.5(d)[e]	46							[74]
51	Ru^{II}	61.6(d)[e]	50.5(d)[e]	45							[73]
52	Rh^{III}	65.4(dd)[e,i]	51.3(d)[e]	45							[73]
53	Ir^{III}	35.3(d)[e]	51.2(d)[e]	41							[73]
54	Ru^{II}	99.3(d)[e]	69.1(d)[e]	36							[74]
55	Rh^{III}	87.2(dd)[e,i]	69.0(d)[e]	39	1.997(4)	1.674	2.293(4)	2.404(3)	121.1(6)	88.3(1)	[75]
56	Ir^{III}	60.9(d)[e]	69.0(d)[e]	32	2.000(8)	1.665	2.263(6)	2.407(5)	122.5(1)	88.6(2)	[73, 75]
57	Cu^{I}	32(br)[e,j]	67.8(m)[e,j]	[j]							[76]

[a] Chemical shifts, coupling constants, bond lengths and angles given in ppm, Hz, Å and deg, respectively; [b] multiplicity of the NMR signals given in parenthesis; [c] average value; [d] in d_6-DMSO; [e] in $CDCl_3$; [f] $|^{2}J_{P,P=S} + {}^{3}J_{P,P'=S}|$; [g] in CD_2Cl_2; [h] measured $^{2+3}J_{P,P}$, but the complexity of the AA'BB' spin system is described in the main text; [i] $^{1}J_{P,Rh}$ = 148 and 139 Hz for **52** and **55**, respectively; [j] P^{III} and P^{V} resonances were not attributed and $J_{P,P}$ coupling constants not given.

5. *N*-substituted mono-sulfide DPPA-type ligands

The mono-sulfide DPPA-type ligands **58**-**61**, substituted on the N atom by pure hydrocarbyl groups [*i.e.* Ph, (*S*)-CHMePh, ^{i}Pr and 1-Naphtyl, respectively], were easily accessible *via* oxidation by an equimolar amount of elemental sulfur of the parent diphosphines (Scheme 20) [77-81]. Interestingly, these mixed P/P=S ligands were isolated without contamination of the bis-sulfide derivatives after work-up. Similarly to **DPPA-S**, the ^{31}P NMR spectra of ligands **58**-**61** exhibited two sharp doublets (AX spin system) in the 52.4-54.5 and 67.5-73.1 ppm regions for the non-equivalent P^{III} and P^{V} nuclei, respectively (Table 6). The solid-state molecular structure of ligand **59**, determined by XRD analysis, revealed a nearly trigonal planar N atom linked asymmetrically to the P^{III} [1.749(4) Å] and P^{V} [1.695(4) Å] atoms. This asymmetry is generally also present, although less pronounced, in the coordination compounds of *N*-substituted/functionalized mono-oxidized DPPA-type ligands.

5.1. Group 10 metal complexes

P,S-chelate palladium (**62**, **64**, **66**, **68**) and platinum (**63**, **65**, **67**, **69**) dichloride complexes of the type [MCl_2{(**58**-**61**)-*P,S*}] were obtained by substitution of the labile ligand(s) in [$MCl_2(L_2)$] [M = Pd, Pt; L_2 = COD, $(PhCN)_2$] precursors with the mixed P/P=S ligands **58**-**61** (Scheme 20) [77, 79-81]. Similarly, the organo-palladium complexes [PdCl(Me){(**59**-**60**)-*P,S*}] (**70**-**71**) were synthesized from [PdCl(Me)(COD)] and the respective ligand (Scheme 20) [82]. Al-Masri and Moussa observed that the reaction between the mixed P/P=S ligand **61** and $[NiCl_2(PPh_3)_2]$ afforded the *P,P*-chelate complex [$NiCl_2${(Ph_2P)N(1-Naphthyl)}-*P,P*], resulting from the desulfurization of the *P*,P=*S* DPPA-type ligand **61** and formation of Ph_3P=S and the corresponding *P,P* ligand [81]. ^{31}P NMR spectroscopy revealed that upon coordination to the Pd^{II} or Pt^{II} centers, the chemical shifts of the *P*Ph_2 doublet are downfield shifted, of *ca*. 40-50 and 10-20 ppm, respectively, compared to the free ligands, while the *P*=S resonances are only slightly affected (Table 6). In all of these d^8 metal complexes, the $^2J_{P,P}$ was found in the same range. The assignment of both P^{III}/P^{V} resonances was facilitated, in the case of the Pt^{II} complexes (**63**, **65**, **67**, **69**), by the presence of typical $^1J_{P,Pt}$ and $^2J_{P=S,Pt}$ satellites due to the couplings of the phosphorus atoms with the ^{195}Pt center (spin = ½). For the organo-palladium complexes **70**-**71**, the *cis*-position of the Me group with respect to the coordinated P atom was assessed by the observation of a characteristic $^3J_{P,H}$ coupling of 3.9 Hz by ^{1}H NMR. Single-crystal XRD analysis on complexes **63**-**65** confirmed the expected square-planar arrangement of the ligands; one mixed *P,S*-chelate and two chlorines, around the Pd^{II} or Pt^{II} metal center. The characteristic P-N, P=S and P-M bond lengths and PNP and SMP angles are very similar in the three complexes (Table 6). The only significant structural differences with respect to the related complex [$PdCl_2${(**46**)-*P,O*}] (**47**, Figure 6) are the P=E and (P=)E-Pd bond lengths (E = O, S) due to a much larger atomic radius for S compared to O.

The two *C,N*-cyclometallated *P,S*-chelate Pd^{II} complexes [Pd{$(C_6H_3$-R'-4)-N=N-$(C_6H_4$-R'-4)-*C,N*}{(**60**)-*P,S*}][PF_6] [R' = H (**72**), OC_6H_{13} (**73**)] were obtained *via* a chlorido-bridge cleavage reaction of [Pd(μ-Cl){$(C_6H_3$-R'-4)-N=N-$(C_6H_4$-R'-4)-*C,N*}]$_2$ with 2 eq. of ligand **60** in the presence of NH_4PF_6 (Scheme 20) [82]. While complexes **72** and **73** may exist as two isomers, their ^{31}P NMR spectra revealed the formation of only one isomer, which exhibited two doublets at *ca*. 98 and 69 ppm, as expected for the non-equivalent P^{III} and P^{V} nuclei, respectively (Table 6). The downfield shift of the *P*Ph_2 resonance in **72** and **73**, compared to the free ligand **60**, is very similar to that observed for the palladium dichloride derivatives (**62**, **64**, **66**, **68**). The arrangement of the *P,S*- and *C,N*-chelate ligands could be unambiguously established by XRD studies for **73**. The σ-bonded C center occupies the position *trans* with respect to the S, as observed in the Pd-Me complexes **70**-**71**. Structurally, the presence of a σ-bonded aryl group on the Pd^{II} center in **73** resulted in the lengthening of the *trans* Pd-S bond compared to the *P,S*-$PdCl_2$ system **64** [2.386(1) *vs*. 2.274(2) Å, Table 6].

Reaction of ligands **59** and **60** with the chlorido-bridged dimers [(η^3-1,3-R^1-R^2-C_3H_3)Pd(μ-Cl)]$_2$ (R^1, R^2 = H, Me or Ph) in the presence of NH_4PF_6 led to the cationic η^3-allyl Pd^{II} complexes [(η^3-1,3-

R^1-R^2-C_3H_3)Pd(**59**-**60**)-*P*,*S*}][PF_6] (**74**-**83**, Scheme 20) [83]. The ^{31}P NMR spectra of the resulting complexes **74**-**83** feature an AX spin system for the non-equivalent P^{III} and P^{V} nuclei, which resonate in the 86-97 and 74-81 ppm regions, respectively (Table 6). In the case of the non-substituted allyl derivatives (R^1 = R^2 = H, **74** and **79**), the allylic symmetry is broken by the mono-sulfide DPPA-type ligands itself, resulting in the observation of; 1) five distinct resonances by ^{1}H NMR, and 2) a dynamic behavior for the H atoms *trans* to the S donor. The NMR spectra of the complexes **74**-**78** are more complicated, because of additional possibility of face-coordinated diastereomeric pairs due the chiral nature of ligand **59**. Mono-substitution of the allyl group by one Me or Ph group led to additional possibilities of *cis*/*trans* arrangement of the latter substituent with respect to the S (or P) donor. The Me derivatives **75** and **80** exist respectively as mixtures of 6 and 4 isomers. Unlike **75** and **80**, the Ph derivatives **76** and **81** exist as mixtures of 4 and 2 isomers, respectively, due to the absence of any *anti*-isomer because of higher steric congestion of Ph *vs*. Me. Bis-substitution of the allyl ligand with two Me in complexes **77** and **82** drives the co-existence of 6 and 3 isomers, respectively. In contrast to the latter complexes, when the allyl ligand is di-substituted with two bulkier Ph groups, only 2 and 1 isomers are observed by solution NMR for complexes **78** and **83**, respectively. In Table 6 are only summarized the ^{31}P NMR data for the *syn*, *trans*-to $P^{III}Ph_2$ (**75**, **76**, **80**, **81**) or *syn*/*syn*-allylic isomers (**77**, **78**, **82**, **83**), which are observed for each complex, however the authors clearly detailed the ^{1}H, ^{13}C and ^{31}P NMR data for all (diastereo)isomers in ref [83]. The solid-state molecular structure of complex **74**, established by XRD analysis, revealed the presence of only one diastereoisomer. The square-planar coordination geometry around the Pd^{II} center is strongly distorted, due to the acute C-Pd-C' angle [67.5(5)°] imposed by the allyl ligand, while the *P*,*S*-chelate allows a P-Pd-S angle of 94.6(8)° closer to the expected 90° (Table 6). Apart from the P-Pd bond length of 2.285(2) Å, which is close to that measured in the **DPPA-O** analog of **74** [**2**: P-Pd = 2.283(2) Å, Table 1], the other characteristic structural parameters of complexes **2** and **74** differ significantly. The latter observation highlights how subtle changes in DPPA-type ligands, *i.e*. *N*-substitution and/or P=E oxidation, can affect the resulting coordination compounds and may influence their reactivity and/or catalytic activity. In this context, *in-situ* generated pre-catalysts based on ligands **59**, **60** and their non-oxidized *P*,*P* parent ligands were evaluated in the allylic alkylation of (*E*)-1-phenyl-2-propenyl acetate with dimethyl malonate (conditions: 1 mol% Pd, 2.5 mol% ligand, 24 h, 25°C) [83]. All complexes exhibited similar activity, *i.e*. complete conversion under the studied conditions, and regio-selectivity, affording 95-97% of the linear product. The authors assumed that this high selectivity is related to steric factors, which favor the nucleophilic substitution to operate on the unsubstituted terminus of the substrate.

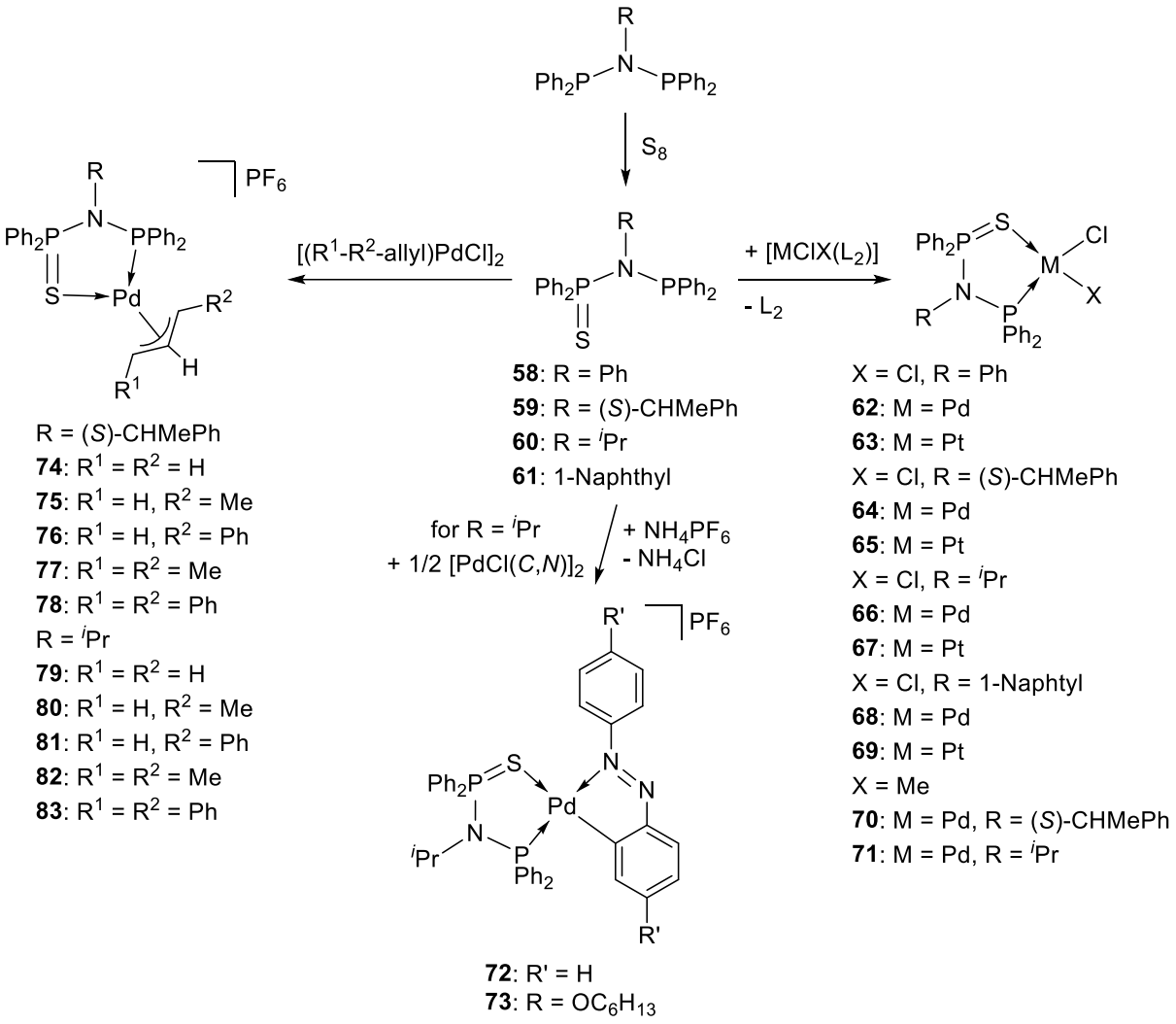

Scheme 20. Mono-sulfide DPPA-type ligands with pure hydrocarbyl *N*-substituents (**58**-**61**) and their Pd^{II} and Pt^{II} complexes (**62**-**83**) [77-83]. Note: R^1-R^2-allyl = η^3-1,3-R^1-R^2-CHCHCH, L_2 = COD or $(PhCN)_2$.

Increasing efforts have been made over the last decades to introduce various chemical functions as *N*-substituent in DPPA-type ligands [27], however the number of examples of mono-oxidized derivatives is rather limited. The presence of an additional donor on the *N*-substituent may result in the formation of polynuclear assemblies (see *e.g.* [4, 7, 84-86]), but the latter can also act as a stabilizing ligand for reactive/unsaturated species during a catalytic cycle. From the adjunction of a suitable *N*-functionalized tail raised the possibility to anchor coordination compounds on solid matrices or on metal surfaces (see *e.g.* [87-91]).

The synthesis of the mono-sulfide *N*-functionalized DPPA-type ligands $(PPh_2)N\{P(S)Ph_2\}(R)$ [R = *o*-(C_6H_4)OMe (**84**), *p*-(C_6H_4)SMe (**85**), $(CH_2)_3$SMe (**89**)] was achieved by reaction of the parent diphosphine ligands with elemental sulfur (Scheme 21) [72, 92, 93]. However, all mono-sulfide ligands

were always contaminated by the bis-sulfide derivatives and could never be isolated in a pure form. While Smith and co-workers used the isolated **84** (*ca*. 90% pure) for the coordination reactions [92], Fliedel, Braunstein and co-workers generated *in-situ* the mono-sulfide ligands **85** and **89**, using 1.5 eq. of sulfur, before addition of 1 eq. of metal precursor, and then removed the unreactive (towards the metals studied) bis-sulfide derivatives formed [93]. Ligands **84**-**85** and **89** exhibited, in their ^{31}P NMR spectra, the awaited two doublets (AX spin system) for the non-equivalent P^{III} and P^{V} nuclei at very similar chemical shifts (*ca*. 54 and 73 ppm, respectively). While the nature of the *N*-substituent did not affect (much) the chemical shift of the P atoms, the $^{2}J_{P,P}$ coupling constant varies much more (**58**-**61**, **84**-**85**, **89**, Table 6). Substitution of the labile COD or $(PhCN)_2$ (L_2) ligands in $[MCl_2(L_2)]$ (M = Pd, Pt) by 1 eq. of the chelating mixed P/P=S ligand led to the formation of the complexes $[MCl_2$(**84**-**85**)-*P*,*S*}] (**86**-**88**, Scheme 21) [92, 93]. Upon coordination to palladium, both P^{III} and P^{V} NMR resonances were downfield shifted, while the coordination to platinum led only to downfield shift of the P^{III} resonance accompanied by the appearance of typical $^{1}J_{P,Pt}$ and $^{2}J_{P=S,Pt}$ satellites (Table 6). The slightly distorted square-planar coordination geometry around the d^8 metal ions was confirmed in the case of **87** and **88** by XRD analysis. The characteristic bond lengths and angles were found in the same ranges as for the Pd^{II} and Pt^{II} complexes of *N*-substituted DPPA-type ligands (**63**-**65**, Table 6).

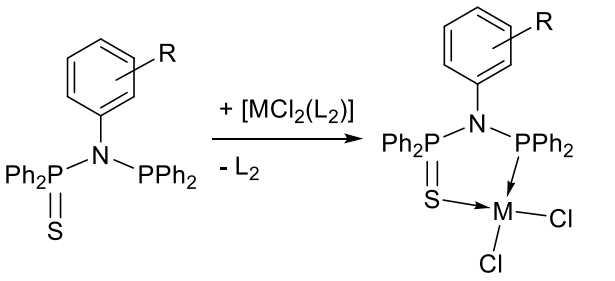

84: R = *o*-OMe
85: R = *p*-SMe

86: M = Pd, R = *o*-OMe
87: M = Pt, R = *o*-OMe
88: M = Pd, R = *p*-SMe

Scheme 21. Synthesis of Pd^{II} and Pt^{II} complexes (**86**-**88**) of mono-sulfide *N*-functionalized DPPA-type ligands (**84**-**85**) [92, 93]. Note: L_2 = COD or $(PhCN)_2$.

Fliedel, Braunstein and co-workers studied the coordination chemistry of the mono-sulfide *N*-thioether functionalized DPPA-type ligands **85** and **89** towards Ni^{II} precursors, with the objective of evaluating the influence of the chelate-ring size (*P*,*P vs. P*,P=*S* chelation) and/or the *N*-substituent on the catalytic performances of the resulting complexes [72, 93]. As anticipated, the 2:1 reaction between the *P*,P=*S*-ligands and $[Ni(NCMe)_6][BF_4]$ afforded the bis-chelate dicationic complexes [Ni{(**85**, **89**)-*P*,*S*}$_2$][BF_4]$_2$ (**90**-**91**) by substitution of the labile MeCN ligands (Scheme 22). Both complexes exhibited two triplets, downfield shifted compared to the free ligands, in their ^{31}P NMR spectra, corresponding to an AA'BB' spin system (Table 6). The solid-state structures of complexes **90**-**91**, established by XRD, confirmed the formation of diamagnetic square-planar Ni^{II} complexes, bis-*P*,*S*-chelated by two ligands

85 or **89** *trans* to each other, respectively. The main structural features of **90** and **91** are very similar to each other and to those of complex **93'**, another *trans* bis-chelate Ni^{II} complex. However, the P-Ni and (P=)S-Ni bond lengths slightly differ from the respective *P*,*S*-$NiCl_2$ species **92** and **93** due to different *trans* influences (Table 6).

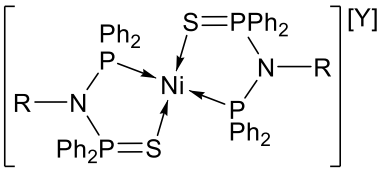

90: R = *p*-(C_6H_4)SMe , Y = $(BF_4)_2$
91: R = $(CH_2)_3$SMe, Y = $(BF_4)_2$
92': R = *p*-(C_6H_4)SMe, Y = $NiCl_4$
93': R = $(CH_2)_3$SMe, Y = $NiCl_4$
94': R = *p*-(C_6H_4)SMe, Y = $NiBr_4$

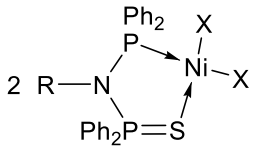

92: R = *p*-(C_6H_4)SMe , X = Cl
93: R = $(CH_2)_3$SMe, X = Cl
94: R = *p*-(C_6H_4)SMe, X = Br

Scheme 22. Ni^{II} complexes (**90**-**94**) of ligands **85** [R = *p*-(C_6H_4)SMe] and **89** [R = $(CH_2)_3$SMe] [72, 93].

The ^{31}P NMR spectrum of the purple material resulting from the stoichiometric reaction between ligand **89** and [$NiCl_2$(COD)] exhibited a broad signal at δ = 86.6 ppm, which contrast to the expected two doublets (AX spin system) for a complex of the type [$NiCl_2${(**89**)-*P*,*S*}] (**93**, Scheme 22). Following detailed investigations by multinuclear NMR, UV/Vis and FT-IR spectroscopic methods and DFT calculations, the authors highlighted the existence of an equilibrium, *via* ligand-redistribution, between the neutral diamagnetic complex [$NiCl_2${(**89**)-*P*,*S*}] (**93**, favored in CH_2Cl_2) and a paramagnetic ion-pair [Ni{(**89**)-*P*,*S*}$_2$][$NiCl_4$] (**93'**, favored in MeOH, Figure 9) [72]. Both isomers can be selectively formed, isolated (*ca*. 90% purity) and characterized depending on the solvent used for the reaction or for the recrystallization (Table 6). A similar behavior was observed by changing the nature of the *N*-substituent (from ligand **89** to **85**) or the halide ligands on the Ni^{II} (from Cl to Br). The resulting complexes (**92**/**92'** and **94**/**94'**) are depicted in Scheme 22 and their spectroscopic and structural data are reported in Table 6 [93]. All the [NiX_2{(**85**, **89**)-*P*,*S*}] complexes (**92**-**94**), unambiguously characterized in the solid-state by XRD, exhibit very similar structural characteristics. They only differ from the Pd^{II} or Pt^{II} analogs by the values of the P-M and (P=)S-M bond lengths ($\Delta\delta$ = *ca*. 0.06 and 0.15 Å, respectively) due to a larger atomic radius for the heavier metals (Table 6). In contrast, the related *P*,*P*-chelate complexes [$NiCl_2$(*P*,*P*)] do not exhibit any dynamic behavior in solution.

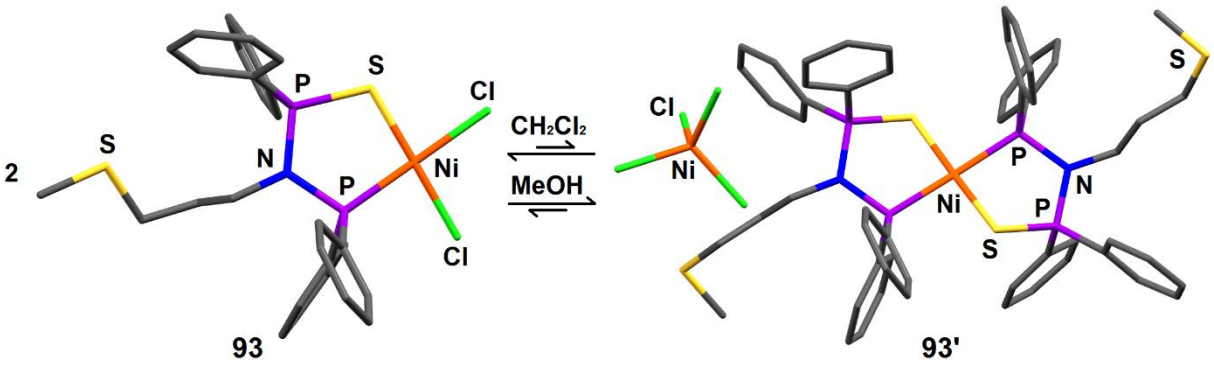

Figure 9. Formula isomer Ni^{II} complexes **93**/**93'** of ligands **89** in equilibrium [72].

Fliedel, Braunstein and co-workers reported that, in the presence of Zn metal, complexes **90** and **91** readily activate the inert C_{sp3}–Cl bonds of dichloromethane at room temperature to afford in high yield the phosphonium ylide derivatives $[Ni((Ph_2P)N\{P(CH_2)Ph_2\}(R)\text{-}P,C)_2][BF_4]_2$ [R = $(CH_2)_3SMe$, *p*-$(C_6H_4)SMe$] [94]. The authors suggested that this reactivity resulted from the reduction of both P^V=S to P^{III} and Ni^{II} to Ni^0 by the Zn reagent.

The influence of the *N*-substituent and chelate ring-size on the catalytic activities of the *P*,*S*-$NiCl_2$ species **92** and **93** and their *P*,*P*-$NiCl_2$ counter-parts in ethylene oligomerization was evaluated and discussed [93]. Using $AlEtCl_2$ as co-catalyst, butene (58-87%) and hexene (11-36%) were formed as major products, with the best productivity of 48 200 g of C_2H_4/((g of Ni) h) or TOF of 101 100 mol of C_2H_4/((mol of Ni) h) being obtained with complex **93**. The catalytic results clearly highlighted that both 1) the chelate-ring size and/or donor set (*P*,*P vs. P*,P=*S*) and 2) the nature of the *N*-substituent [*p*-$(C_6H_4)SMe$ in **85**/**92** *vs*. $(CH_2)_3SMe$ in **89**/**93**] influence the performances of the Ni^{II} pre-catalysts [93]. Although a clear explanation for the different catalytic activities within this series of complexes could not be provided, several studies were conducted in the recent years to rationalize the (pre)catalyst/organoaluminum reagent interaction(s) and to identify potential active species in olefin polymerization catalysis [95].

Table 6. ^{31}P NMR data and characteristic structural parameters of free mono-sulfide DPPA-type ligands (**58**-**61**, **84**-**85**, **89**) and Group 10 metal (+2 oxidation state) complexes **62**-**83**, **86**-**88** and **90**-**95** (Table divisions: free *N*-substituted ligands, corresponding metal complexes, free *N*-functionalized ligands, corresponding metal complexes).[a]

	M^{II}	$\delta(P^{III})$[b]	$\delta(P^{V})$[b]	$^2J_{P,P=S}$	$^1J_{P,Pt}$	$^2J_{P=S,Pt}$	P=S	P-N[c]	P-M	S-M	PNP	SMP	Ref.
58		54.5[d]	72.4[d]	105									[77]
59		52.4[e]	72.0[e]	13			1.955(2)	1.722			124.3(2)		[75, 79]
60		54.4[f]	67.5[f]	63									[78]
61		52.7[e]	73.1[e]	105									[81]
62	Pd	106.2[d]	80.5[d]	57									[77]
63	Pt	76.6[d]	75.4[d]	53	3857	88	2.003(3)	1.706	2.197(2)	2.306(2)	115.4(4)	90.5(8)	[77]
64	Pd	98.0[e]	75.9[e]	48			2.011(3)	1.698	2.214(2)	2.274(2)	116.0(3)	91.2(7)	[79]
65	Pt	70.2[e]	72.7[e]	48	3976	104	2.016(4)	1.712	2.212(3)	2.260(3)	115.1(6)	92.1(1)	[79]
66	Pd	97.3[e]	75.2[e]	51									[80]
67	Pt	69.6[e]	71.6[e]	48	3787	100							[80]
68	Pd	102.9[e]	74.0[e]	59									[81]
69	Pt	72.5[e]	70.1[e]	55	3897								[81]
70	Pd	96.3[f]	70.9[f]	58									[82]
71	Pd	98.6[f]	70.5[f]	58									[82]
72	Pd	97.8[e]	69.1[e]	49									[82]
73	Pd	97.9[e]	69.1[e]	52			1.995(2)	1.697	2.246(1)	2.386(1)	113.7(2)	91.2(1)	[82]
74[g]	Pd	90.0[e]	78.1[e]	82			1.992(3)	1.713	2.285(2)	2.375(2)	110.2(4)	94.6(8)	[83]
75[g]	Pd	90.4[e]	76.5[e]	60									[83]
76[g]	Pd	87.7[e]	74.1[e]	71									[83]
77[g]	Pd	89.2[e]	75.2[e]	82									[83]
78[g]	Pd	92.5[e]	76.5[e]	76									[83]
79	Pd	93.7[e]	78.7[e]	90									[83]
80	Pd	93.6[e]	76.5[e]	73									[83]

81	Pd	93.6[e]	76.5[e]	73									[83]
82	Pd	94.6[e]	76.4[e]	81									[83]
83	Pd	91.7[e]	78.0[e]	76									[83]
84		53.7[e]	73.5[e]	104									[92]
85		55.3[e]	72.4[e]	105									[93]
89		53.9[h]	72.6[h]	86									[72]
86	Pd	78.6[e]	105.7[e]	62									[92]
87	Pt	73.4[e]	73.4[e]	57	3884	110	2.010(2)	1.712	2.203(1)	2.295(1)	116.2(2)	92.5(1)	[92]
88	Pd	80.1[e]	106.7[e]	60			2.004(1)	1.701	2.204(9)	2.309(1)	118.5(2)	90.5(3)	[93]
90	Ni	84.6[h]	105.8[h]	[i]			2.020(4)	1.698	2.198(3)	2.180(3)	114.7(6)	93.2(1)	[93]
91	Ni	86.3[h]	95.6[h]	[i]			2.017(1)	1.685	2.187(8)	2.190(7)	117.3(1)	90.2(3)	[72]
92	Ni	83.8[e,j]					2.004(1)	1.705	2.138(1)	2.163(1)	118.0(2)	94.3(4)	[93]
93	Ni	86.6[e,j]					2.012(2)	1.692	2.139(2)	2.154(2)	118.5(2)	94.1(6)	[72]
93'	Ni	86.3[k]	94.4[k]	[i]			2.017[c]	1.689	2.213[c]	2.185[c]	115.6[c]	91.7[c]	[72]
94	Ni	83.7[e,j]					2.013(1)	1.706	2.144(1)	2.158(1)	118.1(2)	94.8(3)	[93]

[a] Chemical shifts, coupling constants, bond lengths and angles given in ppm, Hz, Å and deg, respectively; [b] appears as doublet unless specified; [c] average value; [d] in $CDCl_3$ or CD_2Cl_2; [e] in $CDCl_3$; [f] in CH_2Cl_2; [g] the ^{31}P NMR data of only one of the two diastereoisomers are given; [h] in CD_2Cl_2; [i] $^{2+3}J_{P,P=S} = {}^{2+3}J_{P',P'=S} = 77.3$ (**90**), 67.5 (**91**), 67.2 (**94'**) Hz, $^{3+4}J_{P,P'=S}$, = 66.3 (**90**), 5.7 (**91**), 7.4 (**94'**) Hz, $^{4}J_{P=S,P'=S} = 76.4$ (**90**), 66.1 (**91**), 66.5 (**94'**) Hz, $^{2}J_{P,P'} = 76.4$ (**90**), 68.1 (**91**), 68.4 (**94'**) Hz; [j] broad singlet due to the fast equilibrium between **92**/**92'**, **93**/**93'** or **94**/**94'**, respectively; [k] in CD_3OD.

5.2. Group 9 metal complexes

Reaction between ligands **58**-**60** and 0.5 eq. of the dimeric precursor [Rh(μ-Cl)(CO)$_2$]$_2$ afforded the mononuclear complexes [RhCl(CO){(**58**-**60**)-*P*,*S*}] (**95**-**97**, Scheme 23) [77, 80]. The *cis* arrangement of the carbonyl ligand with respect to the phosphine donor is evidenced by typical ν(CO) absorption bands in the 1978-1985 cm^{-1} region. The ^{31}P NMR spectrum of **95** exhibits two doublets of doubletsfor the P^{III} and P^{V} atoms, representative of a AMX spin system, at 122.8 ($^2J_{P,P=S}$ = 71.3 Hz, $^1J_{P,Rh}$ = 158.7 Hz) and 76.0 ppm ($^2J_{P=S,Rh}$ = 3.0 Hz), respectively. The NMR data of complexes **96** and **97** followed similar trends (Table 7). The X-ray structure of complex **96** revealed a tetra-coordinated Rh^{I} center in a slightly distorted square-planar geometry, with coordination angles ranging from 87.5(2) to 92.8(7)° [80]. The confirmed *cis* arrangement of the carbonyl ligand with respect to the phosphine donor contrasts with the structure of the Pd^{II} complex **70**, in which the neutral donor (N) is located *trans* to the P donor (see section 5.1 and Scheme 20). The characteristic bond lengths and angles in **96** (Table 7) are comparable to those measured in **73** (similar *P*,*S*, L, X coordination environment, Table 6).

Ligand substitution reaction in [M(μ-Cl)(COD)]$_2$ (M = Rh, Ir) by **59** (2 eq.) led to the formation of the dinuclear chlorido-bridged complexes [M(μ-Cl){(**59**)-*P*,*S*}]$_2$ [M = Rh (**98**), Ir(**99**), Scheme 23], in which ligand **59** acts as a *P*,*S*-chelate [79]. This result strongly contrasts with that observed with **DPPA-O**, which selectively formed complexes [MCl(COD){(**DPPA-O**)-*P*}] (**26**-**27**, Scheme 10), in which the mixed *P*,(P=)*O* ligand acts as a *P*-monodentate donor, highlighting the different reactivity of mono-sulfide *vs*. mono-oxide derivatives of DPPA. The ^{31}P NMR resonances of both P^{III} and P^{V} nuclei were significantly downfield shifted in complexes **98** and **99** compared to the free ligand **59**, and a typical $^1J_{P,Rh}$ of 158 Hz could be observed for **98** (Table 7). Interestingly, while two geometric isomers, *cis* and *trans*, could be formed with the asymmetric ligand **59**, a single isomer was formed for the Rh^{I} complex **98**. In the case of Ir^{I}, although the initial reaction (CH_2Cl_2, RT, 2 h) afforded a single isomer of **99** [δ = 95.1 (P^{III}) and 72.9 (P^{V}) ppm], after five days in $CDCl_3$ a second isomer was formed [δ = 82.0 (P^{III}) and 77.0 (P^{V}) ppm]. The authors could establish that the isomerization is favored by the addition of THF or of a catalytic amount of excess ligand, suggesting the formation of a five-coordinate intermediate, which then undergoes either 1) a pseudo-rotation to exchange the ligand positions or 2) a cleavage of one chlorido-bridge followed by rotation around the M-Cl-M axis before re-formation of the chlorido-bridge. The authors suggested that the back-donation of the bridging Cl to the coordinated P atom should be lower in the case of the *cis* isomer, because both P share the same Cl atom as *trans* ligand. As a consequence, the ^{31}P NMR resonance of the P^{III} nucleus in the *cis* isomer should be at lower field, and the P,P coupling should be greater, compared to the *trans* isomer. It was concluded that the initial product formed was **99**-*cis*, which also exhibited a higher asymmetry in the ν(Ir-Cl) region of the FT-IR spectrum, while the more stable complex is **99**-*trans*.

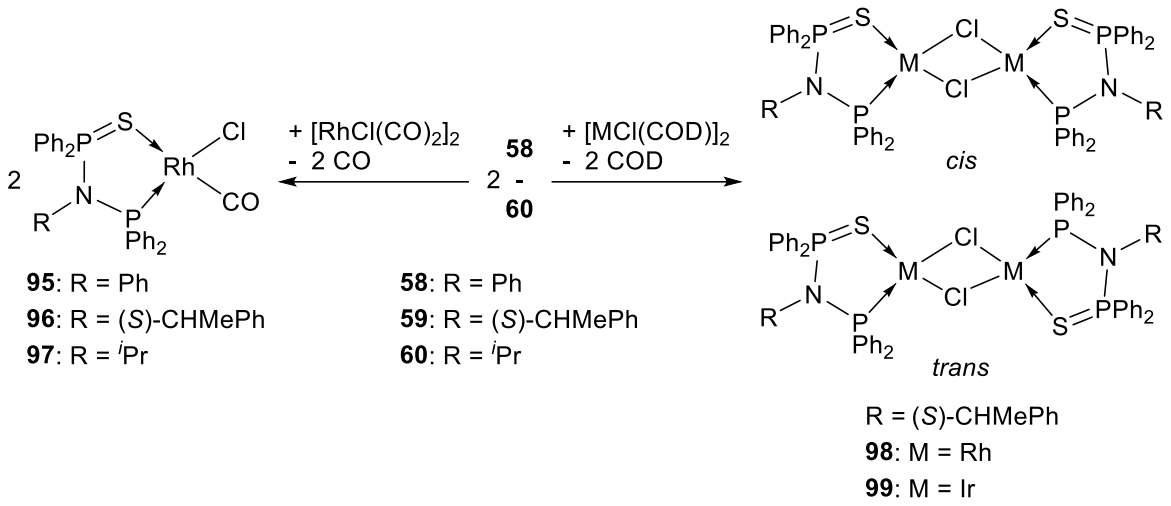

Scheme 23. Synthesis of Rh^{I} and Ir^{I} complexes (**95**-**99**) of mono-sulfide *N*-substituted DPPA-type ligands (**58**-**60**) [77, 79, 80].

The one-pot reaction between [Rh(μ-Cl)(COD)]$_2$, ligand **59** and $NaBF_4$ in a 1:2:2 molar ratio, afforded the mononuclear cationic complex [Rh(COD){(**59**)-*P*,*S*}][BF_4] (**100**), as deduced by EA, multinuclear NMR and FT-IR spectroscopic techniques (Table 7) [75].

Table 7. ^{31}P NMR data and characteristic structural parameters of Group 9 metal complexes **95-100**.[a]

	M	$\delta(P^{III})$[b]	$\delta(P^{V})$[b]	$^{2}J_{P,P=S}$	$^{1}J_{P,M}$	$^{2}J_{P=S,M}$	P=S	P-N[c]	P-M	S-M	PNP	SMP	Ref.
95	Rh^{I}	122.8(dd)[d]	76.0(dd)[d]	71	159	3							[77]
96	Rh^{I}	112.3(dd)[e]	68.5(d)[e]	63	167		1.992(5)	1.72	2.208(5)	2.369(5)	110.1(8)	89.2(2)	[80]
97	Rh^{I}	114.9(dd)[e]	69.2(d)[e]	65	164								[80]
98	Rh^{I}	104.6(dd)[e]	70.9(d)[e]	66	158								[79]
99-*cis*	Ir^{I}	95.1(d)[e]	72.9(d)[e]	66									[79]
99-*trans*	Ir^{I}	82.0(d)[e]	77.0(d)[e]	57									[79]
100	Rh^{I}	103.0(dd)[e]	69.8(d)[e]	66	156								[75]

[a] Chemical shifts, coupling constants, bond lengths and angles given in ppm, Hz, Å and deg, respectively; [b] multiplicity of the NMR signals given in parenthesis; [c] average value; [d] in $CDCl_3$ or CD_2Cl_2; [e] in $CDCl_3$.

5.3. Group 8 metal complexes

Valderrama and co-workers reported several pathways to access the cationic *P*,*S*-chelate complex [(C_6Me_6)RuCl{(**101**)-*P*,*S*}][BF_4] (**102**, Scheme 24) [74]. The latter could be synthesized from the parent neutral complex [(C_6Me_6)$RuCl_2${(**DPPA-S**)-*P*}] (**50**, see section 4 and Scheme 18) by chloride abstraction and *N*-methylation, using $AgPF_6$ and MeI, respectively. Another route involves the *N*-methylation of the neutral species [(C_6Me_6)RuCl{(**DPPA-S$_{-H}$**)-*P*,*S*}], which incorporates the deprotonated mono-sulfide *P*,*S*-chelating ligand derived from DPPA. Finally, complex **102** was readily obtained by chlorido-bridge cleavage reaction of [(C_6Me_6)Ru(μ-Cl)Cl]$_2$ with 2 eq. of the isolated ligand **101**, the latter being obtained *via* oxidation of the corresponding diphosphine [(Ph_2P)$_2$NMe] with elemental sulfur. The ^{31}P NMR spectrum of **102** exhibited the expected two doublets for the non-equivalent P^{III} and P^{V} nuclei, and only the resonance of the P atom directly coordinated to the Ru^{II} center was downfield shifted compared to the free ligand ($\Delta\delta$ = 55.1 ppm, Table 8).

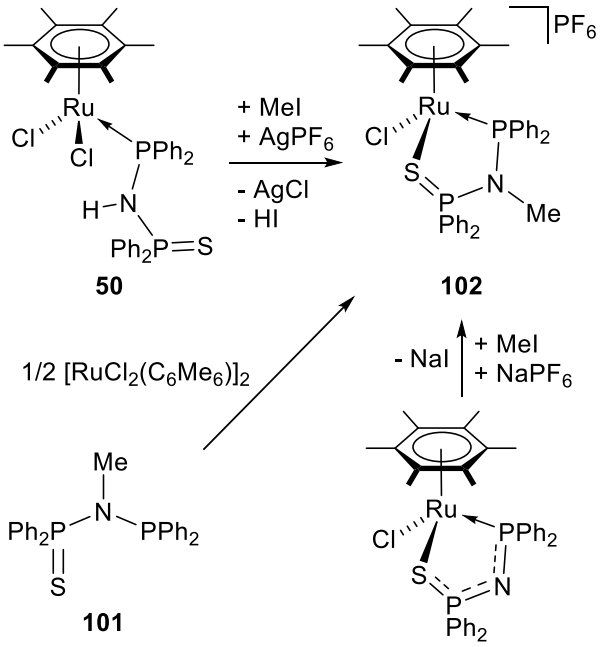

Scheme 24. Synthetic routes to the *P*,*S*-chelate Ru^{II} complex **102** [74].

The piano-stool complexes [Cp^RRuCl{(**58**)-*P*,*S*}] [Cp^R = Cp (**103**), Cp* (**104**)] were readily obtained by substitution of the labile (PPh_3)$_2$ or COD (L_2) ligands in [(Cp^R)RuCl(L_2)] by an equimolar amount of ligand **58** (Scheme 25) [96]. Analysis of the ^{31}P NMR spectra of complexes **103** and **104** revealed a significant influence of the Cp or Cp* ligand on the P resonances of ligand **58**. While in both cases the P^{III} resonance was downfield shifted of *ca*. 70 ppm, the P^{V} resonance was found upfield shifted in **103** (Cp ring, $\Delta\delta$ = 28.7 ppm) and nearly not shifted in **104**, the latter being supported by the more electron donating Cp* ligand ($\Delta\delta$ = 1.5 ppm, Table 8). The authors studied the thermodynamic parameters of the aforementioned ligand substitution reaction, establishing that the reaction with the non-oxidized *P*N(Ph)*P* ligand is more exothermic ($\Delta H_{reaction}$ > by *ca*. 10 kcal.mol^{-1}) than those involving

its mono-oxidized *P*N(Ph)P=*S* (or *Se*) derivatives, both within the Cp and Cp* series. As a result, the *P*,*S*(or *Se*)-chelate complexes are less thermodynamically stable than their *P*,*P*-chelate analogs. Furthermore, the authors observed that the ligand substitution reaction is less exothermic for the Cp*- than the Cp-Ru system, rationalized by the higher electron-donating power of Cp* (*vs*. Cp), which renders the Ru^{II} center more basic, hence less electrophilic, and does not favor the coordination of an additional incoming ligand with greater electron density.

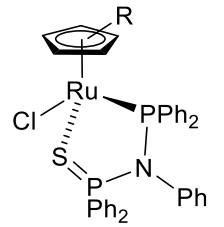

103: R = H_5 (Cp)
104: R = Me_5 (Cp*)

Scheme 25. Piano-stool Ru^{II} complexes (**103**-**104**) of the *P*,*S*-chelate ligand **58** [96].

The stoichiometric reaction between the *N*-substituted mono-sulfide DPPA-type ligands **59**-**60** and $[Ru_3(CO)_{12}]$, in the presence of Me_3NO, afforded the mono-sulfur capped triruthenium clusters $[Ru_3(\mu\text{-}CO)(CO)_7(\mu_3\text{-}S)\{(Ph_2P)_2NR\text{-}P,P\}]$ [R = CHMePh (**105**), ^{i}Pr (**106**), Scheme 26] [80]. In this reaction, the $Ru(0)_3$ core cluster formally undergoes an oxidative addition (of S), while the P^V=S group is reduced (to P^{III}). However, since complexes **105**-**106** no longer contain any mixed P/P=S ligand, they will not be further discussed in the present review. It could be noticed that a similar reactivity was observed with a related P/P=S ligand in which the Ph substituents of the P atoms have been replaced by OPh groups [97].

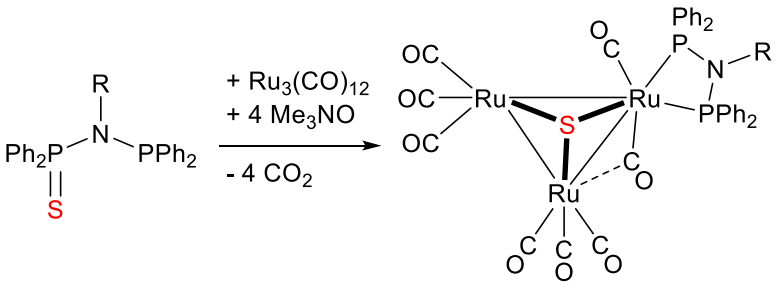

59: R = (*S*)-CHMePh
60: R = ^{i}Pr

105: R = (*S*)-CHMePh
106: R = ^{i}Pr

Scheme 26. Reaction of mono-sulfide DPPA-type ligands **59**-**60** with $[Ru_3(CO)_{12}]$ [80].

Table 8. ^{31}P NMR data of free ligand **101** and metal complexes **102**-**104**.[a]

	M	$\delta(P^{III})^b$	$\delta(P^{V})^b$	$^2J_{P,P=S}$	Ref.
101		53.3	74.7	[c]	[74]
102	Ru^{II}	108.4	75.6	50	[74]
103	Ru^{II}	125.9	46.0	46	[96]
104	Ru^{II}	117.9	76.2	70	[96]

[a] Spectra recorded in $CDCl_3$, chemical shifts and coupling constants given in ppm and Hz, respectively; [b] appears as doublet; [c] not given.

5.4. Group 6 metal complexes

The *P*,*S*-chelate molybdenum(0) and tungsten(0) complexes [$M(CO)_4${(**58**, **61**)-*P*,*S*}] (**105**-**108**) were accessible *via* a ligand substitution reaction in [$M(CO)_4(L_2)$] [M = Mo, W, L_2 = COD, $(Pip)_2$] by an equimolar amount of the mono-sulfide *N*-substituted DPPA-type ligands (**58** and **61**, Scheme 27) [77, 98]. The ^{31}P NMR spectra of the complexes **105**-**108** exhibit all two sharp doublets for the non-equivalent P^{III} and P^{V} nuclei, as expected for an AX spin system, with a *P*,*P*=S coupling constant nearly similar to that of the free ligands (Table 6 and Table 9). While the P^{III} resonance was always found at lower field compared to the free ligands ($\Delta\delta$ = 45-68 ppm), the chemical shift of the P^{V} resonances remained similar for **105**-**106** and was only slightly upfield shifted by *ca*. 6 ppm for **107**-**108**. The assignment of the P^{III} and P^{V} resonances was unambiguously established due to the presence of ^{185}W satellites in **106** and **108** (Table 9).

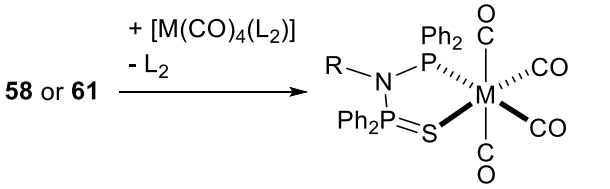

105: M = Mo, R = Ph
106: M = W, R = Ph
107: M = Mo, R = 1-Naphtyl
108: M = W, R = 1-Naphtyl

Scheme 27. Synthesis of Group 6 metal complexes of mono-sulfide *N*-substituted DPPA-type ligands **58** and **61** [77, 98]. Note: L_2 = COD or $(Pip)_2$.

Table 9. ^{31}P NMR data of Group 6 metal complexes **105**-**108**.[a]

	M	$\delta(P^{III})^b$	$\delta(P^{V})^b$	$^2J_{P,P=S}$	$^1J_{P,W}$	$^2J_{P=S,W}$	Ref.
105[c]	Mo^0	115.3	73.0	100			[77]
106[c]	W^0	99.9	73.6	100	258	8	[77]
107[d]	Mo^0	121.0	66.7	100			[98]
108[d]	W^0	105.8	66.9	100	256		[98]

[a] Chemical shifts and coupling constants given in ppm and Hz, respectively; [b] appears as doublet; [c] in $CDCl_3$ or CD_2Cl_2; [d] in $CDCl_3$.

6. DPPA mono-selenide (**DPPA-Se**)

The mono-selenide derivative of DPPA (**DPPA-Se**) could be selectively obtained by the stoichiometric reaction between DPPA and grey selenium (Scheme 28) [71]. The ^{31}P NMR spectrum of **DPPA-Se** exhibits two doublets ($^{2}J_{P,P}$ = 93 Hz, AX spin system) for the non-equivalent P^{III} and P^{V} nuclei at 29.3 and 58.2 ppm, respectively (Table 10). The *P*=S resonance could be unambiguously attributed thanks to the presence of ^{77}Se satellites ($^{1}J_{P,Se}$ = 757 Hz). This property has further been exploited for the assignment of the P^{III} and P^{V} resonances in the **DPPA-Se** complexes and in their *N*-substituted derivatives (see below). The authors highlighted that a controlled "selenide transfer" reaction occurs when mixing **DPPA-Se$_2$** and **DPPA** (1:1 molar ratio), affording solely **DPPA-Se**, whereas no reaction is observed for the **DPPA-S$_2$**/**DPPA** mixture.

Reaction between **DPPA-Se**, *in-situ* generated from DPPA and grey selenium (1:1 molar ratio), and [MCl$_2$(COD)] (M = Pd, Pt), in a 2:1 ligand/metal ratio, afforded the corresponding complexes [M{(**DPPA-Se**)-*P*,*Se*}$_2$][Cl]$_2$ [**109** (Pd), **110** (Pt), Scheme 28] [71]. Noteworthy, the Pd^{II} complex (**109**) was formed as a unique *trans* isomer, while both *cis* and *trans* isomers of the Pt^{II} complex (**110**) were obtained. However, complexes **110**-*trans* and **110**-*cis* present drastically different solubilities; while **110**-*trans* precipitated from the reaction mixture, **110**-*cis* remained in solution and could be further isolated. The ^{31}P NMR spectra of both *trans*-complexes exhibited two triplets for the non-equivalent P^{III} and P^{V} nuclei resulting from an AA'XX' spin system. Upon coordination, the P^{III} resonance is significantly downfield shifted ($\Delta\delta$ = 44-50 ppm) compared to the free ligand, while the P^{V} signals remains in the same region (Table 10). Furthermore, each *P*=Se resonance is flanked by ^{77}Se satellites, and both *P*Ph$_2$ and *P*=Se resonances in **110**-*trans* are flanked by two ^{195}Pt satellites (Table 10). The ^{31}P NMR spectrum of **110**-*cis* reveals a smaller downfield shift for the P^{III} resonance (*ca*. 24 ppm). The solid-state structure of complex **110**-*trans*, determined by XRD analysis, revealed a nearly perfect square-planar coordination geometry around the Pt^{II} center [P-Pt-Se angles = 89.7(1) and 90.3(1)°], composed of two *P*,*Se*-chelating **DPPA-Se** ligands, *trans* to each other. The structure of **110**-*trans* is very similar to that of [Ni{(**DPPA-S**)-*P*,*S*}$_2$][Cl]$_2$ (**49**, section 4 and Table 5), including the presence of N-H•••Cl hydrogen bonds. However and as expected, the P=Se and Se-Pt bond lengths are significantly longer than the P=S and S-Ni ones because of the different atomic radii of the involved elements. In the FT-IR spectra of all above-described d^8 **DPPA-Se** complexes, a characteristic *v*(N-H) absorption band in the 2709-2738 cm^{-1} region could be observed, confirming that no deprotonation of the acidic N-*H* group occurred. Again, the nature of the P=E group was found of importance (Se *vs*. S), because for the **DPPA-S**/Pt couple deprotonation of the ligand occurred (see section 4) [71].

XRD analysis of a crystal resulting from the stoichiometric reaction between the mono-selenide *N*-substituted ligand **120** (see section 7) and NiCl$_2$•6H$_2$O revealed the structure of complex [Ni{(**DPPA-Se$_{-H}$**)-*P*,*Se*}{(**DPPA-Se**)-*P*,*Se*}][Cl] (**111**), incorporating both mono-selenide **DPPA-Se** and its

deprotonated derivative **DPPA-Se**$_{-H}$ [99]. The characteristic structural parameters of **111** are reported in Table 10, but no NMR nor FT-IR data were provided.

Valderrama and co-workers successfully applied the protocol reported for **DPPA-S** (see section 4) to the synthesis of piano-stool Ru^{II}, Rh^{III} and Ir^{III} complexes of **DPPA-Se** [73, 74]. The formation of complexes [(L)MCl_2{(**DPPA-Se**)-*P*}] (**112-115**) (L = C_6Me_6, *p*-Cym), incorporating one **DPPA-Se** ligand coordinated in a *P*-monodentate mode, could be achieved following two different routes. The first path involved; 1) the preliminary synthesis of complexes [(L)$RuCl_2${(**DPPA**)-*P*}] by bridge cleavage reaction of [(L)RuCl(μ-Cl)]$_2$ by 2 eq. **DPPA**, followed by 2) the oxidation of the pendant PPh_2 group with grey selenium (**112-113**, Scheme 28). The second pathway involved the use of isolated **DPPA-Se**, which readily reacted with 0.5 eq. of the dimeric precursors [Cp*MCl(μ-Cl)]$_2$ (M = Rh, Ir) to form the bridged cleaved products (**114-115**, Scheme 28). The ^{31}P NMR spectra of complexes **112-115** are similar to those of their **DPPA-S** analogs (**50-53**, Table 5), with the P^{III} and P^{V} doublet resonances being respectively downfield and upfield shifted, compared to free **DPPA-Se** (Table 10). The P^{V} resonances of complexes **112-115** are flanked by ^{77}Se satellites and the P^{III} resonance of the Rh complex **114** exhibit a typical $^1J_{P,Rh}$ coupling, allowing the unambiguous assignment of each signal. Chloride abstraction reaction in complexes **112** (Ru) and **115** (Ir), using equimolar amounts of $AgPF_6$ or $AgBF_4$, respectively, led to the cationic complexes [(L)MCl{(**DPPA-Se**)-*P*,*Se*}][X] (**116-117**, Scheme 28), in which **DPPA-Se** acts as a *P*,*Se*-chelate ligand. Similar reactivity was observed for the **DPPA-S** derivatives **50**/**54** (Ru) and **53**/**56** (Ir). The ^{31}P NMR spectra of **116-117** exhibited comparable trends to those of **54**, **56**, with downfield shifts of both P^{III} and P^{V} resonances upon cationization and *P*,*Se*-chelation (Table 10) [73, 74]. A lowering of the $^2J_{P,P}$ and $^1J_{P,Se}$ values was also observed. Characteristic ν(N-H) absorption bands (3000-3300 cm^{-1}), and/or N-*H* resonances (δ = 5.95-8.72 ppm) were detected by FT-IR and ^{1}H NMR spectroscopy, respectively, confirming no deprotonation of the acidic N-H group of **112-117**.

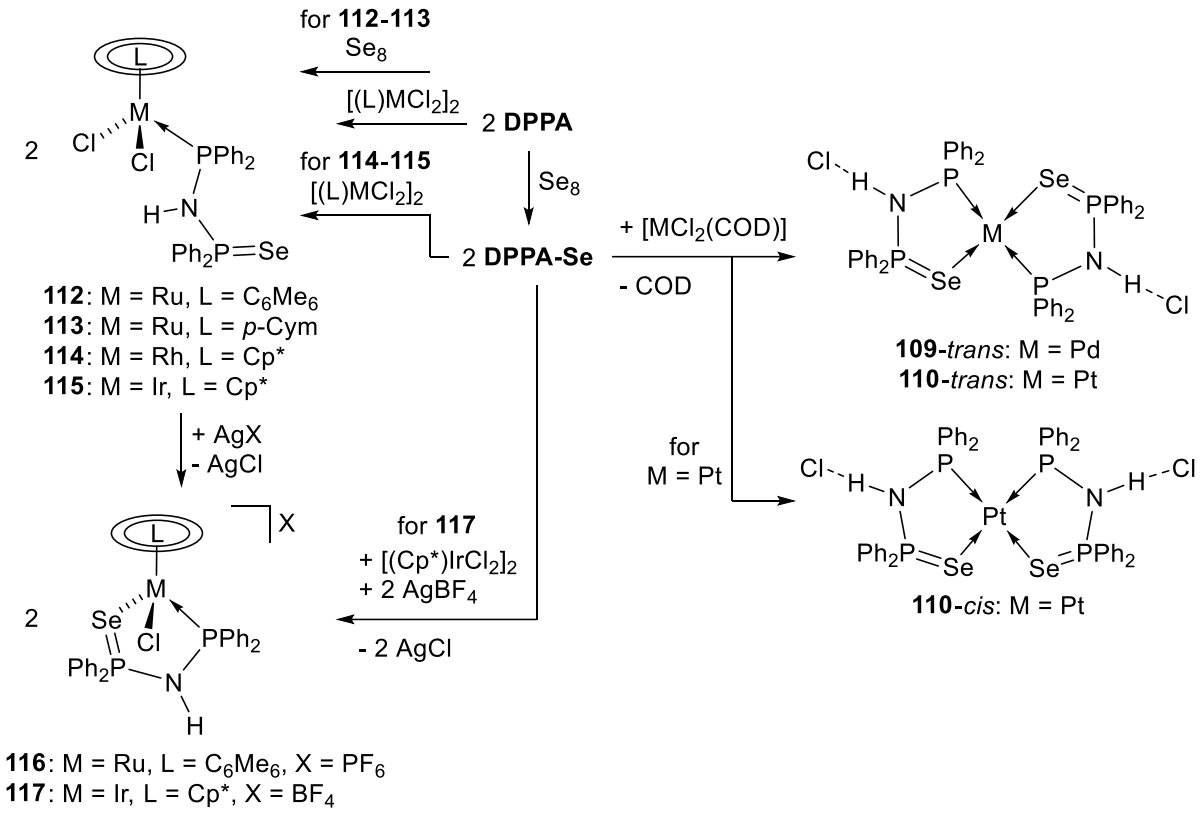

Scheme 28. Synthesis of Group 8-10 metal complexes (**109**-**110** and **112**-**117**) of **DPPA-Se** [71, 73, 74].

The 2:1 reaction between **DPPA-Se** and silver(I) bromide afforded the cationic bis-*P*,*Se*-chelate complex [Ag{(**DPPA-Se**)-*P*,*Se*}$_2$][Br] (**118**) [100]. The Ag^I center in **118** adopts a distorted tetrahedral coordination geometry. The N-*H* group of the **DPPA-Se** ligand in the cation, the Br anion and the EtOH co-crystalized solvent molecule are involved in hydrogen-bonds, forming linear strings, as represented in Figure 10.

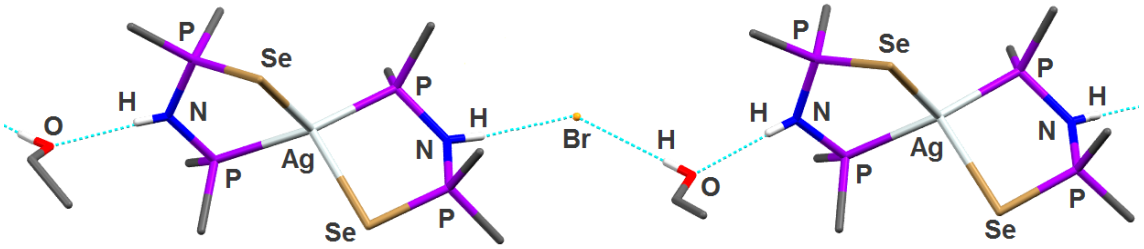

Figure 10. Supramolecular arrangement of complex [Ag{(**DPPA-Se**)-*P*,*Se*}$_2$][Br]•1.5EtOH (**118**•1.5EtOH) formed *via* hydrogen-bonds. Only the N-*H* and EtO*H* hydrogens, and *ipso*-C of the P*Ph* rings are represented for clarity [100].

Table 10. ^{31}P NMR data and characteristic structural parameters of free **DPPA-Se** and metal complexes **109**-**118** (Table divisions: free ligand, Group 10 metals, piano-stool Group 8-9 metal complexes, Group 11 metal).[a]

	M	$\delta(P^{III})$[b]	$\delta(P^{V})$[b]	$^2J_{P,P=Se}$	$^1J_{P,Se}$	$^1J_{P,M}$	$^2J_{P=Se,M}$	P=Se	P-N[c]	P-M	Se-M	PNP	SeMP	Ref.
DPPA-Se		29.3(d)[d]	58.2(d)[d]	93	757									[71]
109-*trans*	Pd^{II}	79.1(t)[e]	59.7(t)[e]	104[f]	523									[71]
110-*trans*	Pt^{II}	73.5(t)[g]	55.7(t)[g]	110[f]	480	2320	74	2.186(3)	1.655	2.300(3)	2.431(2)	122.1(5)	90.3(1)	[71]
110-*cis*	Pt^{II}	63.8(m)[g]	56.2(m)[g]	[h]	480	3270	[h]							[71]
111[i]	Ni^{II}							2.194(7)	1.666	2.206(7)	2.306(4)	120.1(1)	91.3(2)	[99]
112	Ru^{II}	69.3(d)[e]	45.1(d)[e]	48	774									[74]
113	Ru^{II}	62.7(d)[e]	45.3(d)[e]	46	782									[73]
114	Rh^{III}	67.2(dd)[e]	46.1(dd)[e]	46	776	148								[73]
115	Ir^{III}	36.6(d)[e]	45.6(d)[e]	42	780									[73]
116	Ru^{II}	101.7(d)[e]	52.2(d)[e]	37	595									[74]
117	Ir^{III}	53.6(d)[e]	63.8(d)[e]	34	[j]									[73]
118	Ag^{I}	38.7(dd)[k]	62.8(d)[k]	80	[h]	376		2.126[l]	1.685	2.450[l]	2.746[l]	119.1[l]	90.7[l]	[100]

[a] Chemical shifts, coupling constants, bond lengths and angles given in ppm, Hz, Å and deg, respectively; [b] multiplicity of the NMR signals given in parenthesis; [c] average value; [d] in d_6-DMSO; [e] in $CDCl_3$; [f] $|^2J_{P,P=Se} + {}^3J_{P,P'=Se}|$; [g] in CD_2Cl_2; [h] unresolved; [i] the bond lengths and angles given concern the **DPPA-Se** ligand; [j] not reported; [k] in CD_2Cl_2/EtOH; [l] average value.

7. *N*-substituted mono-selenide DPPA-type ligands

The mono-selenide DPPA-type ligands **119**-**121**, substituted on the N atom by a Ph, a chiral (*S*)-CHMePh or a 1-naphtyl group, respectively, were obtained by the equimolar reaction between the parent diphosphines and grey selenium [77, 79, 81]. The ^{31}P NMR data of **119**-**121** are summarized in Table 11. Each ligand exhibits a pair of doublets, consistent with an AX spin system, for the non-equivalent P^{III} and P^{V} nuclei at *ca*. 54 and 72 ppm, respectively. It might be noticed that the P,P coupling in **119**-**121** is strongly dependent on the nature of the *N*-substituent, since aryl groups led to $^{2}J_{P,P}$ of *ca*. 110 Hz (**119**, **121**), while the –CHMePh group afforded a $^{2}J_{P,P}$ of 9 Hz in **120** (Table 11).

Group 10 metal complexes of the mixed *P*/P=*Se* ligands **119**-**121**, of general formula [MCl_2{(**119**-**121**)-*P*,*Se*}] [M = Pd (**122**, **124**, **126**), Pt (**123**, **125**, **127**)], were readily obtained by displacement of the labile COD ligand in [MCl_2(COD)] (M = Pd, Pt) by an equimolar amount of the respective *P*,*Se*-chelate ligand [77, 79, 81]. Upon coordination to the d^8 metal centers, the ^{31}P NMR resonances of the P^{III} and P^{V} donors were respectively downfield and upfield shifted, compared to the free ligands (Table 11). This behavior differs from that of their mono-sulfide analogs **62**-**65**, and **68**-**69** (see section 5 and Table 6), in which the P^{V}(=S) resonance was not significantly shifted. Furthermore, the ^{31}P NMR spectra of **122**-**127** exhibited characteristic ^{77}Se and ^{195}Pt satellites, which allowed the unambiguous assignment of both P^{III} and P^{V} donors. The solid-state structures of both Pd^{II} (**124**) and Pt^{II} (**125**) complexes of the same mixed *P*/P=*Se* ligands **120**, were established by XRD studies. Both structures are very similar, and close to those of their mono-sulfide analogs (**64**-**65**), with the exception, as expected because of the different chalcogen atom radius, of the P=Se and Se-M bond lengths (Table 11 *vs*. Table 6).

Ligand substitution reactions in Group 6 metal precursors of the type [$M(CO)_4(L_2)$] [M = Mo, W, L_2 = COD, $(Pip)_2$] by the mono-selenide DPPA-type ligands **119** and **121**, in a 1:1 ligand/metal molar ratio, afforded the complexes [$M(CO)_4${(**119**, **121**)-*P*,*S*}] (**128**-**131**) [77, 98]. The ^{31}P NMR chemical shifts of the *P*Ph_2 and *P*=Se groups in **128**-**131** were found at lower and higher fields, respectively, compared to the free ligands (Table 11). As for the Group 10 metal complexes (see above), the upfield shift of the *P*=Se resonances in **128**-**131** is much more pronounced than for their corresponding *P*=S analogs (**105**-**108**, Table 9). The structures of complexes **130**-**131**, supported by the same mono-selenide *N*-1-naphtyl-substituted DPPA-type ligand **121**), were determined by single-crystal XRD analysis [98]. The two structures are very similar, with the Mo^0 or W^0 center in a distorted octahedral coordination geometry with the *P*,*Se*-chelate ligand **121** occupying two *cis*-coordination positions. In the structures of metal complexes of mono-oxide or mono-sulfide derivatives, the P^{III}-N bond length is always slightly longer than the P^{V}-N bond, because of stronger delocalization along the N-P=E (E = O, S) moiety, but the bond length difference is $\leq$ 0.05 Å, and therefore average values were reported in the Tables. However, in the case metal complexes of mono-selenide DPPA-type ligands, this bond length difference is greater, up to 0.09 Å in the case of the electron-rich W^0 complex **131** (Table 11 and Figure 11). Two

particular structural features, which might result from steric hindrance around the metal center in **130** and **131**, could be noticed; 1) the two apical CO ligands are not linear and 2) the *N*-aryl group is nearly perfectly orthogonal to the PNP plane (Figure 11), which is not always the case with *N*-aryl DPPA-type ligands [84, 87, 101].

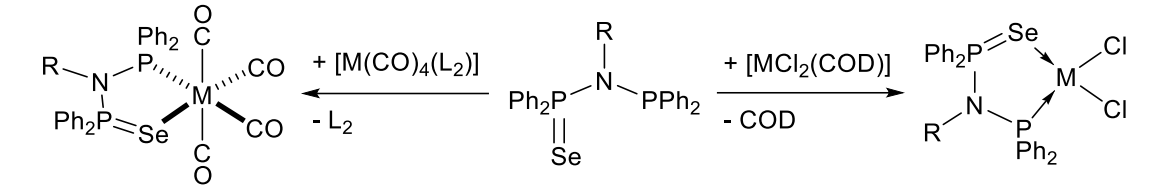

128: M = Mo, R = Ph
129: M = W, R = Ph
130: M = Mo, R = 1-Naphtyl
131: M = W, R = 1-Naphtyl

119: R = Ph
120: R = (*S*)-CHMePh
121: 1-Naphthyl

R = Ph
122: M = Pd
123: M = Pt
R = (*S*)-CHMePh
124: M = Pd
125: M = Pt
X = Cl, R = 1-Naphtyl
126: M = Pd
127: M = Pt

Scheme 29. Mono-selenide DPPA-type ligands with pure hydrocarbyl *N*-substituents (**119**-**121**) and their Group 10 (**122**-**127**) and 6 (**128**-**131**) metal complexes [77, 79, 81, 98]. Note: L_2 = COD or $(pip)_2$.

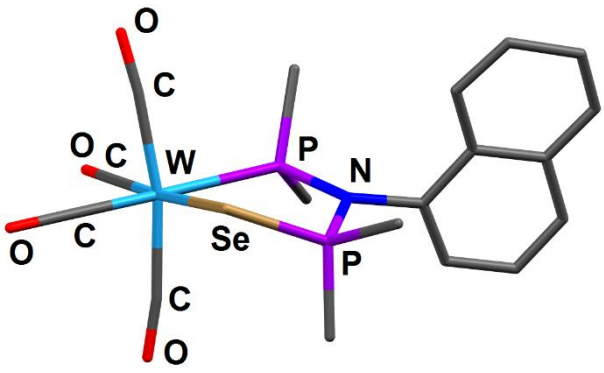

Figure 11. Solid-state structure of the complex $[W(CO)_4\{$(**121**)-*P*,*Se*$\}]$ (**131**). The H atoms are omitted and only the *ipso*-C of the P*Ph* rings are represented for clarity [98].

Group 9 metal complexes of the mixed *P*/P=*Se* ligands **119**, **120** and **132** were synthesized following the same procedures that afforded their *P*,*S*-analogs (see section 5.2 and Scheme 23). The complex [RhCl(CO){(**119**, **132**)-*P*,*Se*}] (**133**-**134**) were obtained *via* chlorido-bridge cleavage and CO substitution in the $[Rh(\mu\text{-Cl})(CO)_2]_2$ dimeric precursor with 2 eq. of **119** or **132** (Scheme 30) [77, 102]. The chlorido-bridged $[M(\mu\text{-Cl})\{$(**120**)-*P*,*Se*$\}]_2$ [M = Rh (**136**), Ir(**137**)] dimers were formed after substitution of the labile COD ligands in the $[M(\mu\text{-Cl})(COD)]_2$ (M = Rh, Ir) precursors with 2 eq. of **120** (Scheme 30) [79]. The ^{31}P NMR spectra of complexes **133** and **134** exhibited the expected two doublets of doublets for each of the non-equivalent P^{III} and P^{V} nuclei, resulting from $^1J_{P,P}$, $^1J_{P,Rh}$ and $^2J_{P=S,Rh}$ couplings, which were significantly downfield and upfield shifted, respectively, compared to the free

ligands (Table 11) [77, 102]. The FT-IR spectra of **132** and **134** showed each a *v*(CO) absorption band at 1981 cm^{-1}, consistent with the *cis* arrangement of the carbonyl ligand with respect to the phosphine donor, similarly to its *P*/P=*S* analog (**95**). The square-planar geometry around the Rh^{I} metal center in **134**, composed of one *P*,*Se* ligand **132**, one CO ligand and one Cl atom was confirmed by XRD analysis. The characteristic structural parameters in **134** were closely related to its *P*,*S* analog (**96**, Table 7), however the presence of the larger Se atom (*vs*. S) engendered greater P=Se, Se-Rh, PNP and SeRhP values (Table 11). Oxidative addition (OA) of MeI to complex **134** yielded the Rh^{III} acyl complex [RhClI{C(O)Me}{(**132**)-*P*,*Se*}] (**135**), *via* its corresponding unisolable alkyl intermediate (**135'**), as depicted in Scheme 30 [102]. The ^{31}P NMR data of **135** were very similar to those of its parent Rh^{I} complex **134** (Table 11). However, the formation of the acyl group in **135** was supported by; 1) a new ^{1}H NMR singlet at δ = 2.81 ppm, and 2) a $\nu(CO)_{acyl}$ absorption band at 1717 cm^{-1} in its FT-IR spectrum, replacing the $\nu(CO)_{terminal}$ in **134** (see above). Noteworthy, complex **134** undergoes the OA slower (4.5 times) than its mono-selenide DPPM analog [RhCl(CO)((Ph$_2$P)CH$_2${P(Se)Ph$_2$}-*P*,*Se*)], and this phenomenon was attributed to a higher nucleophilicity of the latter (*vs*. **134**). Both mono-selenide DPPA-type and DPPM Rh^{I} complexes described above were evaluated in carbonylation of methanol and performed better than the reference catalyst $[RhI_2(CO)_2]^-$. Complex **134** showed higher activity [42.4% yield, TON = 901 (mol of product/mol of Rh)] and selectivity (35.2% methyl acetate, 7.2% acetic acid) than its mono-selenide DPPM analog [102].

The chlorido-bridged structure of complexes [M(μ-Cl){(**120**)-*P*,*Se*}]$_2$ **136** (Rh) and **137** (Ir), along with the non-equivalent donor set in ligand **120** (*P*,P=*Se*), led to the coexistence of two isomers (1:1 approx. ratio) after five hours reaction time [79]. However, the ratio evolved with time and, after three days, a 4:1 ratio in favor of the isomers resonating at higher field and exhibiting the lower P,P and P,Rh coupling constants was reached. These observations clearly illustrate the non-innocent influence of the P=E (E = O, S, Se) group, because the Rh^{I} complex **98** (*P*,*S* ligand **59**, section 5.2) was only obtained as a single isomer, while its *P*,*Se* counterpart **136** exists in two forms. The ^{31}P NMR data for both isomers are summarized in Table 11. However, a conclusive assignment to the *cis* and *trans* forms could not be provided. The proposed mechanism for the isomerization is the same as for the *P*,P=*S* analogous Ir complex **99** (see section 5.2).

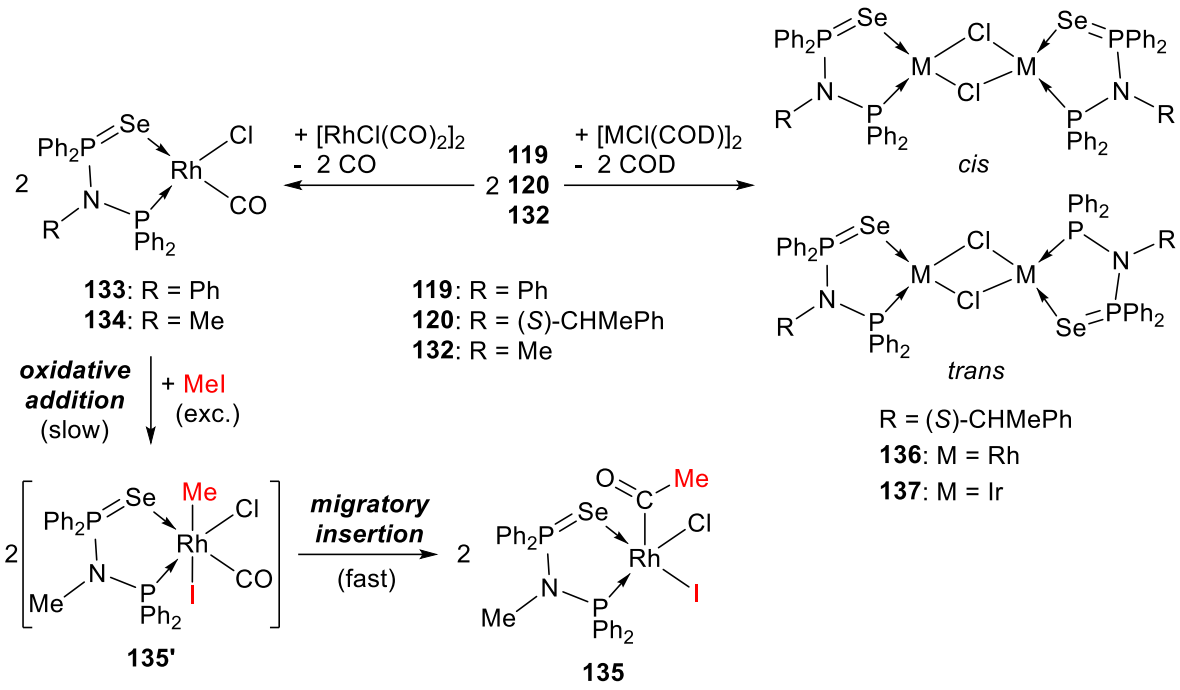

Scheme 30. Synthesis of Group 9 metal complexes (**133-137**) of mono-selenide *N*-substituted DPPA-type ligands (**119**, **120** and **132**) [77, 79, 102].

Balakrishna, Nolan and co-workers reported the synthesis of piano-stool Ru^{II} complexes [Cp^{R}RuCl{(**119**)-*P*,*Se*}] [Cp^{R} = Cp (**138**), Cp* (**139**)], following the same procedure as for their *P*,*S*-analogs (**103-104**, section 5.3) [96]. The ^{31}P NMR spectra of the *P*,*Se*-chelate complexes **135-136** exhibited two doublets for the non-equivalent P^{III} and P^{V} nuclei (AX spin system), significantly downfield and upfield shifted, respectively, compared to the free ligand **119** (Table 11). Both chemical shifts and P,P coupling constants in **135-136** were closely related to their analogous *P*,*S* complexes **103-104** (Table 8). The enthalpies of COD substitution by ligand **119** in the reaction leading to **138** and **139** followed the same trends as for **103-104** (see section 5.3) [96].

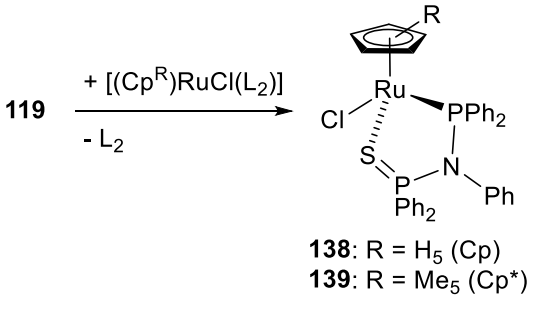

Scheme 31. Piano-stool Ru^{II} complexes (**138-139**) of the *P*,*Se*-chelate ligand **119** [96]. Note: L_2 = COD or $(PPh_3)_2$.

Reaction between the *N*-^{i}Pr substituted DPPA-type mono-selenide ligand [(PPh$_2$)N{P(Se)Ph$_2$}(^{i}Pr)] **137** and [Ru$_3$(CO)$_{12}$] (1:1 molar ratio), in the presence of Me$_3$NO, afforded a mixture of several products [97]. Four products could be isolated and identified by NMR and/or XRD, and in all of them the Ph$_2$P^{V}=Se group was converted/reduced into Ph$_2$P^{III}. The Se atom was transferred to the Ru$_3$ or Ru$_4$ core, resulting in the formation of clusters [Ru$_4$(μ-CO)(CO)$_8$(μ_4-S)$_2${(Ph$_2$P)$_2$N^{i}Pr)-*P*,*P*}] (**138**, major product) and [Ru$_3$(CO)$_7$(μ_3-S)$_2${(Ph$_2$P)$_2$N^{i}Pr)-*P*,*P*}] (**139a-b**, as two isomers, Scheme 32). The other reaction product was tentatively formulated as a diruthenium complex supported by a bridging P,P ligand. However, clusters **138-139** no longer contain any mixed P/P=Se ligand and therefore do not belong to the topic of this review.

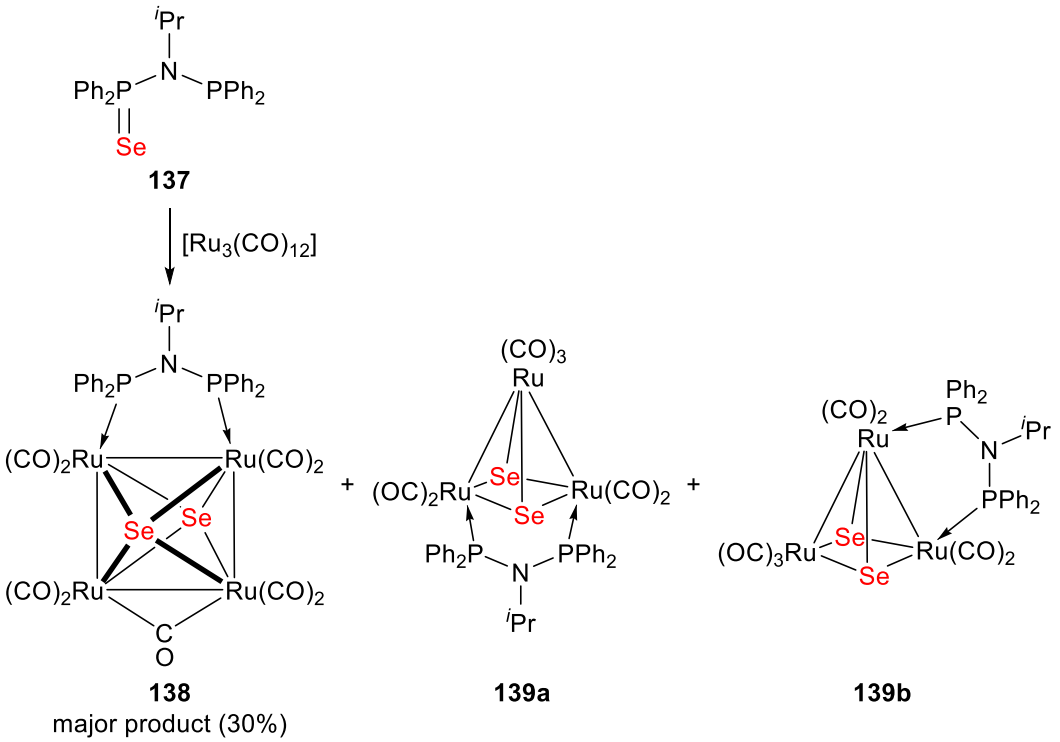

Scheme 32. Reaction of mono-selenide DPPA-type ligands **137** with [Ru$_3$(CO)$_{12}$] [97].

Table 11. ^{31}P NMR data and characteristic structural parameters of free *N*-substituted mono-selenide DPPA-type ligands (**119**-**121**, **132**, **137**) and metal complexes **122**-**131**, **133**-**139** (Table divisions: free ligands, Group 10, 6, 9, 8 metals).[a]

	M	$\delta(P^{III})^b$	$\delta(P^{V})^b$	$^2J_{P,P=Se}$	$^1J_{P,Se}$	$^1J_{P,M}$	$^2J_{P=Se,M}$	P=Se	P^{III}-N	P^{V}-N	P-M	Se-M	PNP	SeMP	Ref.
119		55.1(d)[c]	72.1(d)[c]	110	767										[77]
120		53.1(d)[d]	70.4(d)[d]	9	757										[79]
121		52.9(d)[d]	73.2(d)[d]	112	765										[81]
132		55.7(d)[d]	76.1(d)[d]	96	760										[102]
137		132.5(d)[d]	60.0(d)[d]	102	750										[97]
122	Pd^{II}	111.2(d)[c]	67.6(d)[c]	66	578										[77]
123	Pt^{II}	80.8(d)[c]	61.4(d)[c]	59	554	3918	93								[77]
124	Pd^{II}	103.4(d)[d]	62.7(d)[d]	57	546			2.164(2)	1.723(9)	1.683(7)	2.218(3)	2.377(1)	116.4(4)	92.9(8)	[79]
125	Pt^{II}	73.3(d)[d]	57.8(d)[d]	53	512	3897	110	2.129(3)	1.719(1)	1.688(1)	2.152(3)	2.369(1)	116.5(6)	92.4(9)	[79]
126	Pd^{II}	107.7(d)[d]	64.7(d)[d]	60	583										[81]
127	Pt^{II}	76.7(d)[d]	60.0(d)[d]	60	568	3980									[81]
128	Mo^0	120.3(d)[c]	60.5(d)[c]	112	674										[77]
129	W^0	103.6(d)[c]	60.1(d)[c]	112	661	259									[77]
130	Mo^0	126.7(d)[d]	57.9(d)[d]	112	684			2.145(2)	1.764(5)	1.681(4)	2.523(2)	2.696(8)	120.0(3)	83.4(4)	[98]
131	W^0	110.0(d)[d]	57.1(d)[d]	112	672	258		2.143(2)	1.769(6)	1.676(6)	2.499(2)	2.686(9)	120.0(3)	84.1(5)	[98]
133	Rh^I	126.8(dd)[c]	64.7(dd)[c]	79	602	168	1								[77]
134	Rh^I	119.1(dd)[d]	66.4(dd)[d]	72	481	170		2.153(1)	1.717(4)	1.654(4)	2.201(1)	2.464(6)	122.1(2)	92.4(3)	[102]
135	Rh^{III}	117.0(dd)[d]	68.4(dd)[d]	41		169									[102]
136a	Rh^I	108.7(dd)[d]	59.0(dd)[d]	75	553	158									[79]
136b	Rh^I	93.4(dd)[d]	50.3(dd)[d]	70	556	146									[79]
137a	Ir^I	88.2(d)[d]	51.8(d)[d]	72	551										[79]
137b	Ir^I	85.7(d)[d]	58.6(d)[d]	68	550										[79]
138	Ru^{II}	126.0(d)[d]	42.9(d)[d]	47	710										[96]
139	Ru^{II}	121.8(d)[d]	62.5(d)[d]	81	682										[96]

[a] Chemical shifts, coupling constants, bond lengths and angles given in ppm, Hz, Å and deg, respectively; [b] multiplicity of the NMR signals given in parenthesis; [c] $CDCl_3$ or CD_2Cl_2; [d] in $CDCl_3$.

8. Conclusion

The present review highlights the versatility of the coordination chemistry of mono-oxidized **DPPA**, incorporating one $P^{III}Ph_2$ and one Ph_2P^V=O, =S or =Se donor, and their *N*-substituted derivatives, with pure hydrocarbyl or including an additional chemical function. The presence of a hard O donor in **DPPA-O** favors a *P*-monodentate coordination mode with Group 9 and 10 metal complexes. In contrast, the presence of the softer sulfur or selenide donors in **DPPA-S** or **DPPA-Se** and their *N*-substituted derivatives led, under similar conditions, to the formation of mono- or bis-*P,S* or *P,Se*-chelate complexes. However, formation of *P,O*-chelate species with **DPPA-O** can be promoted by halide abstraction in neutral metal halide complexes. The asymmetry in the donor set in mono-oxidized DPPA-type (*P*,P=*E*, with E = O, S, Se) ligands, compared to their parent diphosphine (*P,P*) ligands, also triggered original reactivity. As a result, *P*,P=*S*-chelate nickel(II) dihalide complexes suffer a solvent-induced isomerization *via* ligand-redistribution, while their *P,P*-chelate analogs are totally inert. Noteworthy, the reaction of **DPPA** with a Re=O precursor led to the oxidation of the ligand *via* transfer of the O atom to form a **DPPA-O** Re complex. In contrast, the reaction of mono-S or -Se DPPA-type ligands with $Ru_3(CO)_{12}$ led to the reduction of P^V=S (or Se) moiety and transfer of the S (or Se) atom to form *P,P*-supported (μ_3-S)-Ru_3 or (μ_4-S)$_2$-Ru_4 clusters. Metal complexes of mono-oxidized DPPA-type ligands found applications in catalytic oligomerization of ethylene, allylic alkylation or carbonylation of methanol.

9. Acknowledgments

We gratefully acknowledge the Centre National de la Recherche Scientifique (CNRS) and the Institut Universitaire de France (IUF) for funding.

10. References

[1] T. Appleby, J.D. Woollins, Coord. Chem. Rev. 235 (2002) 121-140.
[2] P. Bhattacharyya, J.D. Woollins, Polyhedron 14 (1995) 3367-3388.
[3] M.S. Balakrishna, V.S. Reddy, S.S. Krishnamurthy, J.F. Nixon, J.C.T.R. Burkett St. Laurent, Coord. Chem. Rev. 129 (1994) 1-90.
[4] A. Ghisolfi, C. Fliedel, P. de Frémont, P. Braunstein, Dalton Trans. 46 (2017) 5571-5586.
[5] V.W.-W. Yam, V.K.-M. Au, S.Y.-L. Leung, Chem. Rev. 115 (2015) 7589-7728.
[6] H. Schmidbaur, A. Schier, Angew. Chem. Int. Ed. 54 (2015) 746-784.
[7] V. Rosa, C. Fliedel, A. Ghisolfi, R. Pattacini, T. Avilés, P. Braunstein, Dalton Trans. 42 (2013) 12109-12119.
[8] H. Schmidbaur, A. Schier, Chem. Soc. Rev. 41 (2012) 370-412.
[9] V.W.-W. Yam, K.M.-C. Wong, Chem. Commun. 47 (2011) 11579-11592.
[10] S. Sculfort, P. Braunstein, Chem. Soc. Rev. 40 (2011) 2741-2760.
[11] S. Sculfort, P. Croizat, A. Messaoudi, M. Bénard, M.-M. Rohmer, R. Welter, P. Braunstein, Angew. Chem. Int. Ed. 48 (2009) 9663-9667.
[12] Z. Chen, N. Zhao, Y. Fan, J. Ni, Coord. Chem. Rev. 253 (2009) 1-20.
[13] H. Schmidbaur, A. Schier, Chem. Soc. Rev. 37 (2008) 1931-1951.
[14] V.W.-W. Yam, K.K.-W. Lo, Chem. Soc. Rev. 28 (1999) 323–334.
[15] P. Buchwalter, J. Rose, P. Braunstein, Chem. Rev. 115 (2015) 28-126.

[16] C.G. Oliveri, P.A. Ulmann, M.J. Wiester, C.A. Mirkin, Acc. Chem. Res. 41 (2008) 1618-1629.
[17] P. Braunstein, J. Organomet. Chem. 689 (2004) 3953-3967.
[18] P. Braunstein, F. Naud, Angew. Chem. Int. Ed. 40 (2001) 680-699.
[19] C.S. Slone, D.A. Weinberger, C.A. Mirkin, Prog. Inorg. Chem. 48 (1999) 233.
[20] J.I. van der Vlugt, Eur. J. Inorg. Chem. 2012 (2012) 363-375.
[21] P. Espinet, K. Soulantica, Coord. Chem. Rev. 193-195 (1999) 499-556.
[22] A. Bader, E. Lindner, Coord. Chem. Rev. 108 (1991) 27-110.
[23] J. Gopalakrishnan, Appl. Organomet. Chem. 23 (2009) 291-318.
[24] Z. Fei, P.J. Dyson, Coord. Chem. Rev. 249 (2005) 2056-2074.
[25] M. Witt, H.W. Roesky, Chem. Rev. 94 (1994) 1163-1181.
[26] J.D. Woollins, J. Chem. Soc., Dalton Trans. (1996) 2893-2901.
[27] C. Fliedel, A. Ghisolfi, P. Braunstein, Chem. Rev. 116 (2016) 9237-9304.
[28] C. Fliedel et al., Manuscript in preparation.
[29] T.Q. Ly, J.D. Woollins, Coord. Chem. Rev. 176 (1998) 451-481.
[30] C. Silvestru, J.E. Drake, Coord. Chem. Rev. 223 (2001) 117–216.
[31] V.V. Grushin, Chem. Rev. 104 (2004) 1629-1662.
[32] M.B. Smith, A.M.Z. Slawin, J.D. Woollins, Polyhedron 15 (1996) 1579-1583.
[33] P. Bhattacharyya, A.M.Z. Slawin, M.B. Smith, J.D. Woollins, Inorg. Chem. 35 (1996) 3675-3682.
[34] P. Loxq, E. Manoury, R. Poli, E. Deydier, A. Labande, Coord. Chem. Rev. 308 (2016) 131-190.
[35] N. Miyaura, A. Suzuki, Chem. Rev. 95 (1995) 2457-2483.
[36] J.K. Stille, Angew. Chem. Int. Ed. 25 (1986) 508-524.
[37] T.W. Lyons, M.S. Sanford, Chem. Rev. 110 (2010) 1147-1169.
[38] O. Daugulis, H.-Q. Do, D. Shabashov, Acc. Chem. Res. 42 (2009) 1074-1086.
[39] F. Speiser, P. Braunstein, L. Saussine, Acc. Chem. Res. 38 (2005) 784-793.
[40] V.C. Gibson, S.K. Spitzmesser, Chem. Rev. 103 (2003) 283-315.
[41] S.D. Ittel, L.K. Johnson, M. Brookhart, Chem. Rev. 100 (2000) 1169-1203.
[42] M. Albrecht, G. van Koten, Angew. Chem. Int. Ed. 40 (2001) 3750-3781.
[43] J.A. Labinger, Chem. Rev. (2016) 10.1021/acs.chemrev.1026b00583.
[44] A. Furstner, P.W. Davies, Angew. Chem. Int. Ed. 46 (2007) 3410-3449.
[45] I. Brassat, W. Keim, S. Killat, M. Mothrath, P. Mastrorilli, C.F. Nobile, G.P. Suranna, J. Mol. Catal. A: Chem. 157 (2000) 41-58.
[46] A.M.Z. Slawin, M.B. Smith, J.D. Woollins, J. Chem. Soc., Dalton Trans. (1996) 4567-4573.
[47] M.B. Smith, A.M.Z. Slawin, Inorg. Chim. Acta 299 (2000) 172-179.
[48] A.M.Z. Slawin, M.B. Smith, J.D. Woollins, J. Chem. Soc., Dalton Trans. (1996) 1283-1293.
[49] M.R.J. Elsegood, M.B. Smith, S.H. Dale, Acta Crystallogr. Sect. C: Cryst. Struct. Commun. 63 (2007) m7-m9.
[50] R. Malacea, R. Poli, E. Manoury, Coord. Chem. Rev. 254 (2010) 729-752.
[51] X. Cui, K. Burgess, Chem. Rev. 105 (2005) 3272-3296.
[52] H.-U. Blaser, C. Malan, B. Pugin, F. Spindler, H. Steiner, M. Studer, Adv. Synth. Catal. 345 (2003) 103-151.
[53] Y. Park, Y. Kim, S. Chang, Chem. Rev. (2017) 10.1021/acs.chemrev.1026b00644.
[54] G. Song, F. Wang, X. Li, Chem. Soc. Rev. 41 (2012) 3651-3678.
[55] D.A. Colby, R.G. Bergman, J.A. Ellman, Chem. Rev. 110 (2010) 624-655.
[56] R.W. Wegman, A.G. Abatjoglou, A.M. Harrison, J. Chem. Soc., Chem. Commun. (1987) 1891-1892.
[57] A.M.Z. Slawin, M.B. Smith, J.D. Woollins, J. Chem. Soc., Dalton Trans. (1996) 4575-4581.
[58] C.M. Thomas, G. Süss-Fink, Coord. Chem. Rev. 243 (2003) 125-142.
[59] G. Lamb, M. Clarke, A.M.Z. Slawin, B. Williams, L. Key, Dalton Trans. (2007) 5582–5589.
[60] Y. Yang, J. Lan, J. You, Chem. Rev. (2017) 10.1021/acs.chemrev.1026b00567.
[61] P.B. Arockiam, C. Bruneau, P.H. Dixneuf, Chem. Rev. 112 (2012) 5879-5918.
[62] B. Marciniec, Coord. Chem. Rev. 249 (2005) 2374-2390.
[63] R. Noyori, T. Ohkuma, Angew. Chem. Int. Ed. 40 (2001) 40-73.
[64] R. Noyori, S. Hashiguchi, Acc. Chem. Res. 30 (1997) 97-102.
[65] C.-L. Sun, B.-J. Li, Z.-J. Shi, Chem. Rev. 111 (2011) 1293-1314.

[66] A. Correa, O. Garcia Mancheno, C. Bolm, Chem. Soc. Rev. 37 (2008) 1108-1117.
[67] C. Bolm, J. Legros, J. Le Paih, L. Zani, Chem. Rev. 104 (2004) 6217-6254.
[68] J. Parr, M.B. Smith, M.R.J. Elsegood, J. Organomet. Chem. 664 (2002) 85-93.
[69] R. Rossi, L. Marvelli, A. Marchi, L. Magon, V. Bertolasi, V. Ferretti, J. Chem. Soc., Dalton Trans. (1994) 339-345.
[70] A.M.Z. Slawin, J.D. Woollins, Q. Zhang, J. Chem. Soc., Dalton Trans. (2001) 621-632.
[71] P. Bhattacharyya, A.M.Z. Slawin, D.J. Williams, J.D. Woollins, J. Chem. Soc., Dalton Trans. (1995) 3189-3194.
[72] A. Ghisolfi, C. Fliedel, V. Rosa, R. Pattacini, A. Thibon, K. Yu. Monakhov, P. Braunstein, Chem. Asian J. 8 (2013) 1795-1805.
[73] M. Valderrama, R. Contreras, P. Muñoz, M.P. Lamata, D. Carmona, F.J. Lahoz, S. Elipe, L.A. Oro, J. Organomet. Chem. 633 (2001) 182-188.
[74] M. Valderrama, R. Contreras, V. Arancibia, P. Muñoz, Bol. Soc. Chil. Quim. 45 (2000) 227-235.
[75] E. Simon-Manso, M. Valderrama, P. Gantzel, C.P. Kubiak, J. Organomet. Chem. 651 (2002) 90-97.
[76] T. Tsukuda, R. Miyoshi, A. Esumi, A. Yamagiwa, A. Dairiki, K. Matsumoto, T. Tsubomura, Inorg. Chim. Acta 384 (2012) 149-153.
[77] M.S. Balakrishna, R. Klein, S. Uhlenbrock, A.A. Pinkerton, R.G. Cavell, Inorg. Chem. 32 (1993) 5676-5681.
[78] R.P. Kamalesh Babu, K. Aparna, S.S. Krishnamurthy, M. Nethaji, Phosphorus, Sulfur Silicon Relat. Elem. 103 (1995) 39-53.
[79] J.W. Faller, J. Lloret-Fillol, J. Parr, New J. Chem. 26 (2002) 883-888.
[80] K. Raghuraman, S.S. Krishnamurthy, M. Nethaji, J. Organomet. Chem. 669 (2003) 79-86.
[81] H.T. Al-Masri, Z. Moussa, Z. Anorg. Allg. Chem. 642 (2016) 914-920.
[82] S.K. Mandal, S.S. Krishnamurthy, M. Nethaji, Indian J. Chem. 42A (2003) 2422-2426.
[83] S.K. Mandal, G.A. Nagana Gowda, S.S. Krishnamurthy, C. Zheng, S. Li, N.S. Hosmane, J. Organomet. Chem. 676 (2003) 22-37.
[84] C. Fliedel, V. Rosa, A. Falceto, P. Rosa, S. Alvarez, P. Braunstein, Inorg. Chem. 54 (2015) 6547-6559.
[85] C. Fliedel, V. Rosa, A. Falceto, P. Rosa, S. Alvarez, P. Braunstein, Inorg. Chem. 55 (2016) 12100-12100.
[86] C. Fliedel, R. Pattacini, P. Braunstein, J. Clust. Sci. 21 (2010) 397-415.
[87] C. Fliedel, V. Faramarzi, V. Rosa, B. Doudin, P. Braunstein, Chem. Eur. J. 20 (2014) 1263-1266.
[88] B. Lin, Z. Liu, M. Liu, C. Pan, J. Ding, H. Wu, J. Cheng, Catal. Commun. 8 (2007) 2150-2152.
[89] T. Posset, F. Rominger, J. Blümel, Chem. Mater. 17 (2005) 586-595.
[90] F. Schweyer-Tihay, P. Braunstein, C. Estournès, J.L. Guille, B. Lebeau, J.-L. Paillaud, M. Richard-Plouet, J. Rosé, Chem. Mater. 15 (2003) 57-62.
[91] P. Braunstein, H.-P. Kormann, W. Meyer-Zaika, R. Pugin, G. Schmid, Chem. Eur. J. 6 (2000) 4637-4646.
[92] K.G. Gaw, M.B. Smith, A.M.Z. Slawin, New J. Chem. 24 (2000) 429-435.
[93] A. Ghisolfi, C. Fliedel, V. Rosa, K. Yu. Monakhov, P. Braunstein, Organometallics 33 (2014) 2523-2534.
[94] A. Ghisolfi, F. Condello, C. Fliedel, V. Rosa, P. Braunstein, Organometallics 34 (2015) 2255-2260.
[95] S. Dagorne, C. Fliedel, Top. Organomet. Chem. 41 (2013) 125-171.
[96] M.S. Balakrishna, R. Panda, D.C. Smith Jr., A. Klaman, S.P. Nolan, J. Organomet. Chem. 599 (2000) 159-165.
[97] T.S. Venkatakrishnan, S.S. Krishnamurthy, M. Nethaji, J. Organomet. Chem. 690 (2005) 4001-4017.
[98] H.T. Al-Masri, Z. Moussa, A. Fazal, M. Fettouhi, Z. Anorg. Allg. Chem. 640 (2014) 469-475.
[99] N. Levesanos, I. Stamatopoulos, C.P. Raptopoulou, V. Psycharis, P. Kyritsis, Polyhedron 28 (2009) 3305-3309.
[100] J.D.E.T. Wilton-Ely, A. Schier, H. Schmidbaur, J. Chem. Soc., Dalton Trans. (2001) 3647-3651.
[101] C. Fliedel, V. Rosa, B. Vileno, N. Parizel, S. Choua, C. Gourlaouen, P. Rosa, P. Turek, P. Braunstein, Inorg. Chem. 55 (2016) 4183−4198.

[102] D.K. Dutta, J.D. Woollins, A.M.Z. Slawin, D. Konwar, M. Sharma, P. Bhattacharyya, S.M. Aucott, J. Organomet. Chem. 691 (2006) 1229-1234.